Inorg. Chem. **2006**, *45*, 370–385

Synthesis and Characterization of Ruthenacarborane Complexes Incorporating Chelating *N*-Donor Ligands: Unexpected Luminescence from the Complex [3-CO-3,3-{κ^2-$Me_2N(CH_2)_2NMe_2$}-*closo*-3,1,2-$RuC_2B_9H_{11}$]

Paul A. Jelliss,* Justin Mason, Jamie M. Nazzoli, Justin H. Orlando, and Albert Vinson

Department of Chemistry, Saint Louis University, St. Louis, Missouri 63103

Nigam P. Rath

Department of Chemistry and Biochemistry, University of Missouri−St. Louis, St. Louis, Missouri 63128

Michael J. Shaw

Department of Chemistry, Box 1652, Southern Illinois University Edwardsville, Edwardsville, Illinois 62026

Received August 26, 2005

A synthetic methodology using double carbonyl substitution of the starting tricarbonyl complex [3,3,3-$(CO)_3$-*closo*-3,1,2-$RuC_2B_9H_{11}$] (**1**) with 2 mol equiv of the reagent Me_3NO has been employed to afford ruthenacarborane complexes with chelating *N*-donor ligands. Three of these complexes, [3-CO-3,3-{κ^2-4,4′-R_2-2,2′-$(NC_5H_3)_2$}-*closo*-3,1,2-$RuC_2B_9H_{11}$] (**3a**, R = H; **3b**, R = $(CH_2)_8Me$; **3c**, R = Bu^t), comprise 2,2′-bipyridyl ligands with hydrogen, *n*-nonyl, or *t*-butyl groups in the 4,4′-positions of the rings, respectively. Photophysical analysis revealed no substantial luminescent activity, but the complexes are electrochemically active, undergoing sequential (reversible and quasi-reversible) one-electron reductions, the second of which likely precipitating a ligand displacement. Cyclic voltammetry (CV) experiments revealed an irreversible one-electron oxidation ($E_{pa} \approx 0.9$ V) in MeCN, on the other hand, followed by rapid CO substitution by the solvent and reversible secondary reduction ($E_{1/2} \approx 0.1$ V). The primary redox couple became quasi-reversible in CH_2Cl_2, and spectroelectrochemical analysis of complex **3c** provided evidence of a *closo* → *isocloso* structural modification upon oxidation. An analogue of these complexes employing the TMEDA (*N*,*N*,*N*′,*N*′-tetramethylethylenediamine) ligand, [3-CO-3,3-{κ^2-$Me_2N(CH_2)_2NMe_2$}-*closo*-3,1,2-$RuC_2B_9H_{11}$] (**4**), was synthesized using the same methodology. Cyclic voltammetric measurements displayed a reversible metal-based one-electron oxidation whether in CH_2Cl_2 or MeCN, with no indication of subsequent CO substitution or a similar *closo* → *isocloso* adjustment. Complex **4** was unexpectedly weakly luminescent (λ_{em} = 360 nm) in THF (tetrahydrofuran) at ambient temperatures, demonstrating a more intense phosphorescent emission in MeTHF (2-methyltetrahydrofuran) glass at 77 K (λ_{em} = 450 nm, τ_{450} = 0.77 ms). The X-ray crystallographic structures of complexes **3a** and **4** are reported along with spectroscopic IR, NMR (^1H, ^{13}C, ^{11}B), UV–vis absorption, EPR, and CV data.

Introduction

The photophysical and electrochemical behavior of the class of ubiquitous 2,2′-bipyridyl ruthenium(II) complexes are well understood,[1,2] and applications in artificial photosynthesis,[3] photoinduced electron transfer,[4] and semiconductor fabrication[5] have been exhaustively pursued. Despite this comprehensive research, avenues leading to the synthesis and analysis of ruthenium complexes incorporating both carborane and 2,2′-bipyridyl ligands have yet to be explored. Stone et al. have reported the quantitative synthesis of [3,3,3-$(CO)_3$-*closo*-3,1,2-$RuC_2B_9H_{11}$] (**1**),[6] and the studies of its reactions have focused on CO substitution and primary functionaliza-

* To whom correspondence should be addressed. E-mail: jellissp@slu.edu.

10.1021/ic051463e CCC: $33.50
Published on Web 11/17/2005

Chart 1. Molecular Structures of Complexes **1**−**4**

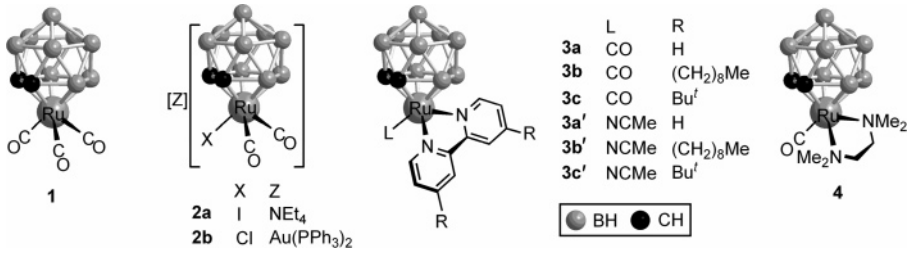

tion at the metal center, with subsequent secondary reactivity at metal-adjacent boron vertexes being frequently observed. Thus, the complex salt $[NEt_4][3\text{-I-}3,3\text{-}(CO)_2\text{-}closo\text{-}3,1,2\text{-}RuC_2B_9H_{11}]$ (**2a**) (Chart 1) has been treated with $AgBF_4$ in THF (tetrahydrofuran) to yield a labile neutral species $[3,3\text{-}(CO)_2\text{-}3\text{-(THF)-}closo\text{-}3,1,2\text{-}RuC_2B_9H_{11}]$, which undergoes reactions with 2-electron donors to give simple adducts $[3,3\text{-}(CO)_2\text{-}3\text{-L-}closo\text{-}3,1,2\text{-}RuC_2B_9H_{11}]$ (L = alkenes, amines, internal alkynes, isonitriles, phosphines).[6,7] Reactions with terminal alkynes, on the other hand, have lead to insertion of rearranged vinylidene ligands into multiple cage B−H bonds adjacent to the metal center.[7a] Reactivity has been investigated with Group 6 metal alkylidynes and Groups 8 and 9 cyclopentadienide complexes, yielding a host of novel di- and trimetallic RuM (M = Mo, W, Fe, Ru, Rh) species with unusual coordination modes involving bridging alkylidyne and/or carborane ligands.[8] We demonstrate herein the further development of the ruthenacarborane complex **1** by introduction of chelating *N*-donor ligands such as 2,2′-bipyridyl and examine the electronic structure of the new complexes through electrochemical and photophysical measurements.

Results and Discussion

Synthesis and Characterization of the Neutral Ruthenacarboranes. Our initial investigations engaged complex **2a** as a potential precursor to 2,2′-bipyridyl adducts. Indeed, treatment of this salt with 2,2′-bipyridyl in MeCN in the presence of 1 mol equiv of Me_3NO led to the formation and isolation of the complex $[3\text{-CO-}3,3\text{-}\{\kappa^2\text{-}2,2'\text{-}(NC_5H_4)_2\}\text{-}closo\text{-}3,1,2\text{-}RuC_2B_9H_{11}]$ (**3a**). However, our attention turned to the parent complex **1** itself, leading to the discovery that reaction with the same reagent (2,2′-bipyridyl) in the same solvent, but with 2 mol equiv of Me_3NO, ultimately resulted in the formation of the same complex, **3a**, in a yield comparable with that for the combined two steps. The same synthetic methodology has been applied to the formation and isolation of the analogous complexes $[3\text{-CO-}3,3\text{-}\{\kappa^2\text{-}4,4'\text{-}R_2\text{-}2,2'\text{-}(NC_5H_3)_2\}\text{-}closo\text{-}3,1,2\text{-}RuC_2B_9H_{11}]$ (**3b**, R = $(CH_2)_8Me$; **3c**, R = Bu^t) using the ligands 4,4′-R_2-2,2′-bipyridyl. All complexes **3** were purified by column chromatography on silica gel and recrystallization from CH_2Cl_2/hexanes to give yellow microcrystalline solids. Despite the presence of strong donor ligands on the metal center, all complexes, either in the solid state or in solution, were stable on the open bench under air. All three complexes displayed a single ν_{max}(CO) absorption in their IR spectra (Table 1, 1961−1966 cm^{-1}) with precise frequencies correlating with the strength of σ-donor substituent in the 4,4′ position of the 2,2′-bipyridyl rings, i.e., decreasing in the order H > $(CH_2)_8Me$ > Bu^t. The increased level of electron density on the metals in complexes **3** is reflected in the ample decrease in ν_{max}(CO) values as compared with the parent tricarbonyl complex **1** (2114, 2058 cm^{-1}).[6] The NMR spectra (Table 2) are in

(1) (a) Hicks, C.; Ye, G. Z.; Levi, C.; Gonzales, M.; Rutenburg, I.; Fan, J. W.; Helmy, R.; Kassis, A.; Gafney, H. D. *Coord. Chem. Rev.* **2001**, *211*, 207. (b) Shan, B. Z.; Zhao, Q.; Goswami, N.; Eichhorn, D. M.; Rillema, D. P. *Coord. Chem. Rev.* **2001**, *211*, 117. (c) Balzani, V.; Juris, A. *Coord. Chem. Rev.* **2001**, *211*, 97. (d) Lee, W. Y. *Mikrochim. Acta* **1997**, *127*, 19.

(2) (a) Gafney, H. D.; Adamson, A. W. *J. Am. Chem. Soc.* **1972**, *94*, 8238. (b) Demas, J. N.; Adamson, A. W. *J. Am. Chem. Soc.* **1973**, *95*, 5159; **1971**, *93*, 1800. (c) Bock, C. R.; Meyer, T. J.; Whitten, D. G. *J. Am. Chem. Soc.* **1974**, *96*, 4710. (d) Young, R. C.; Meyer, T. J.; Whitten, D. G. *J. Am. Chem. Soc.* **1975**, *97*, 4781. (e) Bock, C. R.; Meyer, T. J.; Whitten, D. G. *J. Am. Chem. Soc.* **1975**, *97*, 2909.

(3) (a) Meyer, T. J. *Acc. Chem. Res.* **1989**, *22*, 163. (b) Meyer, T. J. *Carbon Dioxide Fixation and Reduction in Biological and Model Systems*; Proceedings of the Royal Swedish Academy of Sciences, Nobel Symposia; Brändén, C.-I., Schneider, G., Eds.; Oxford University Press: Oxford, 1994; Chapter 14, pp 211−224. (c) Meijer, M. D.; Van Klink, G. P. M.; Van Koten, G. *Coord. Chem. Rev.* **2002**, *230*, 141. (d) Durr, H.; Bossmann, S. *Acc. Chem. Res.* **2001**, *34*, 905. (e) Sun, L. C.; Hammarstrom, L.; Akermark, B.; Styring, S. *Chem. Soc. Rev.* **2001**, *30*, 36. (f) Gust, D.; Moore, T. A.; Moore, A. L. *Acc. Chem. Res.* **2001**, *34*, 40. (g) Bouas-Laurent, H.; Castellan, A.; Desvergne, J. P.; Lapouyade, R. *Chem. Soc. Rev.* **2000**, *29*, 43.

(4) (a) Meyer, T. J. *Intramolecular, Photochemical Electron and Energy Transfer, Photochemical Processes in Organized Molecular Systems*; Proceedings of the Memorial Conference for the late Professor Shigeo Tazuke, Yokohama, Japan, Sept 22−24, 1990; Honda, K., Ed.; North-Holland, Elsevier: Amsterdam, 1991; pp 133−143. (b) Meyer, T. J. *Pure Appl. Chem.* **1990**, *62*, 1003. (c) Qu, P.; Thompson, D. W.; Meyer, G. J. *Langmuir* **2000**, *16*, 4662. (d) Keene, F. R. *Coord. Chem. Rev.* **1997**, *166*, 121. (e) Schoonover, J. R.; Bignozzi, C. A.; Meyer, T. J. *Coord. Chem. Rev.* **1997**, *165*, 239. (f) Rillema, D. P.; Blanton, C. B.; Shaver, R. J.; Jackman, D. C.; Boldaji, M.; Bundy, S.; Worl, L. A.; Meyer, T. J. *Inorg. Chem.* **1992**, *31*, 1600.

(5) (a) Grätzel, M. *Curr. Opin. Colloid Interface Sci.* **1999**, *4*, 314. (b) Kalyanasundaram, K.; Grätzel, M. *Coord. Chem. Rev.* **1998**, *177*, 347. (c) Gerfin, T.; Grätzel, M.; Walder, L. *Prog. Inorg. Chem.* **1997**, *44*, 345. (d) Hagfeldt, A.; Grätzel, M. *Chem. Rev.* **1995**, *95*, 49. (e) Bak, T.; Nowotny, J.; Rekas, M.; Sorrell, C. C. *Int. J. Hydrogen Energy* **2002**, *27*, 991. (f) Burgeth, G.; Kisch, H. *Coord. Chem. Rev.* **2002**, *230*, 41. (g) Rajeshwar, K.; de Tacconi, N. R.; Chenthamarakshan, C. R. *Chem. Mater.* **2001**, *13*, 2765. (h) Kelly, C. A.; Meyer, G. J. *Coord. Chem. Rev.* **2001**, *211*, 295. (i) Garcia, C. G.; deLima, J. F.; Iha, N. Y. M. *Coord. Chem. Rev.* **2000**, *196*, 219.

(6) (a) Anderson, S.; Mullica, D. F.; Sappenfield, E. L.; Stone, F. G. A. *Organometallics* **1995**, *14*, 3516. (b) Behnken, P. E.; Hawthorne, M. F. *Inorg. Chem.* **1984**, *23*, 3420. (c) Siedle, A. R. *J. Organomet. Chem.* **1975**, *90*, 249.

(7) (a) Anderson, S.; Mullica, D. F.; Sappenfield, E. L.; Stone, F. G. A. *Organometallics* **1996**, *15*, 1676. (b) Jeffery, J. C.; Jelliss, P. A.; Psillakis, E.; Rudd, G. E. A.; Stone, F. G. A. *J. Organomet. Chem.* **1998**, *562*, 17.

(8) (a) Anderson, S.; Jeffery, J. C.; Liao, Y.-H.; Mullica, D. F.; Sappenfield, E. L.; Stone, F. G. A. *Organometallics* **1997**, *16*, 958. (b) Ellis, D. D.; Farmer, J. M.; Malget, J. M.; Mullica, D. R.; Stone, F. G. A. *Organometallics* **1998**, *17*, 5540. (c) Jeffery, J. C.; Jelliss, P. A.; Rudd, G. E. A.; Sakanishi, S.; Stone, F. G. A.; Whitehead, J. *J. Organomet. Chem.* **1999**, *582*, 90.

Table 1. Analytical and Physical Data

compound	color	yield %	ν_{max}(CO)[a] cm^{-1}	analysis[b]/% C	H	N
[3-CO-3,3-{κ^2-2,2′-$(NC_5H_4)_2$}-*closo*-3,1,2-$RuC_2B_9H_{11}$] **3a**	yellow-orange	23	1966s	37.4 (37.2)	4.6 (4.8)	6.7 (6.2)
[3-CO-3,3-{κ^2-4,4′-$((CH_2)_8Me)_2$-2,2′-$(NC_5H_3)_2$}-*closo*-3,1,2-$RuC_2B_9H_{11}$] **3b**	yellow	21	1963s	55.7 (55.6)	8.3 (8.3)	4.1 (4.2)
[3-CO-3,3-{κ^2-4,4′-Bu^t_2-2,2′-$(NC_5H_3)_2$}-*closo*-3,1,2-$RuC_2B_9H_{11}$] **3c**	yellow	48	1961s	47.1 (47.6)	6.7 (6.7)	5.2 (5.3)
[3-CO-3,3-{κ^2-$Me_2N(CH_2)_2NMe_2$}-*closo*-3,1,2-$RuC_2B_9H_{11}$] **4**	orange	44	1942s	28.9 (28.6)	7.2 (7.2)	7.3 (7.4)

[a] Measured in CH_2Cl_2 at 298 K; medium-intensity bands observed at ca. 2550 cm^{-1} in the spectra of all compounds are due to B−H absorptions. [b] Calculated values are given in parentheses.

Table 2. ^1H, ^{13}C, and ^{11}B NMR Data[a]

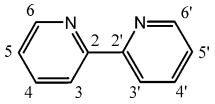

compd	$^1H/\delta$	$^{13}C/\delta$[b]	$^{11}B/\delta$[c]
3a	8.71 (d, 2 H, $H^{6,6'}$, $^3J_{HH}$ = 5), 8.09 (d, 2 H, $H^{3,3'}$, $^3J_{HH}$ = 8), 7.81 (dd, 2 H, $H^{4,4'}$, $^3J_{HH}$ = 8, 8), 7.24 (dd, 2 H, $H^{5,5'}$, $^3J_{HH}$ = 5, 8), 2.88 (s, 2 H, cage CH)	206.7 (CO), 156.4 ($C^{2,2'}$), 156.1 ($C^{6,6'}$), 139.5, 127.5, 124.3 ($C^{3,3'}$, $C^{4,4'}$, $C^{5,5'}$), 45.6 (br, cage C)	0.6 (s, 1 B), −4.9 (s × 2, 3 B), −6.2 (s, 2 B), −18.2 (s × 2, 3 B)
3b	8.85 (d, 2 H, $H^{6,6'}$, $^3J_{HH}$ = 6), 8.27 (d, 2 H, $H^{3,3'}$, $^3J_{HH}$ = 2), 7.40 (dd, 2 H, $H^{5,5'}$, $^3J_{HH}$ = 2, 6), 3.16 (s, 2 H, cage CH), 2.83 (t, 4 H, $CH_2(CH_2)_7Me$, $^3J_{HH}$ = 7), 1.74 (dd, 4 H, $CH_2CH_2(CH_2)_6Me$, $^3J_{HH}$ = 7 and 7), 1.36 (m, 8 H, $CH_2CH_2(CH_2)_2(CH_2)_4Me$), 1.28 (m, 16 H, $CH_2CH_2(CH_2)_2(CH_2)_4Me$), 0.87 (t, 6 H, $CH_2(CH_2)_7Me$, $^3J_{HH}$ = 6)	206.5 (CO), 156.4 ($C^{6,6'}$), 156.2 ($C^{2,2'}$), 155.4 ($C^{4,4'}$), 127.6, 124.2 ($C^{5,5'}$, $C^{3,3'}$), 45.6 (br, cage CH), 35.9, 32.7, 30.9, 30.2, 30.1, 30.0, 29.8, 23.5 ($(CH_2)_8Me$), 14.5 ($(CH_2)_8Me$)	0.8 (s, 1 B), −4.8 (s × 2, 3 B), −6.3 (s, 2 B), −18.2 (s × 2, 3 B)
3c	8.90 (d, 2 H, $H^{6,6'}$, $^3J_{HH}$ = 7), 8.40 (d, 2 H, $H^{3,3'}$, $^3J_{HH}$ = 3), 7.58 (dd, 2 H, $H^{5,5'}$, $^3J_{HH}$ = 3, 7), 3.16 (s, 2 H, cage CH), 1.45 (s, 18 H, CMe_3)	207.7 (CO), 164.9 ($C^{6,6'}$), 156.8 ($C^{2,2'}$), 156.1 ($C^{4,4'}$), 125.2, 122.0 ($C^{5,5'}$, $C^{3,3'}$), 45.9 (br, cage CH), 37.0 (CMe_3), 31.3 (CMe_3)	1.1 (s, 1 B), −4.6 (s × 2, 3 B), −6.1 (s, 2 B), −18.1 (s × 2, 3 B)
4	3.52 (s, 2 H, cage CH), 3.01, 2.85 (m × 2, 4 H, CH_2), 2.96, 2.66 (s × 2, 12 H, NMe_2)	201.8 (CO), 64.7, 58.7, 53.4 (CH_2NMe_2), 49.6 (br, cage CH)	−0.3 (s, 1 B), −3.1 (s, 1 B), −8.1 (s, 2 B), −11.2 (s, 2 B), −17.4 (s, 2 B), −22.8 (s, 1 B)

[a] Chemical shifts (δ) in ppm, coupling constants (J) in Hz, measurements at 298 K in CD_3CN. [b] ^1H-decoupled, chemical shifts are positive to high frequency of $SiMe_4$. [c] ^1H-decoupled, chemical shifts are positive to high frequency of $BF_3{\cdot}OEt_2$ (external).

accord with structures of C_s symmetry in solution, with a mirror plane bisecting the molecule through the metal, CO ligand, apical boron, and the midpoint of the cage C−C connectivity. Thus, all three complexes **3** displayed single resonances for cage C−H protons (δ 2.88 (**3a**), 3.16 (**3b**,**c**)) in their respective ^1H NMR spectra. The same spectra also revealed the expected aromatic resonances for the 2,2′-bipyridyl ligands, with integrations appropriate for a bipyridyl/carborane ratio of 1:1. A resonance at δ 1.45 is readily ascribed to the equivalent *t*-butyl groups of complex **3c**, while the hydrocarbon protons of the similarly equivalent *n*-nonyl groups in complex **3b** occur in the region δ 0.87−2.83, in agreement with previously characterized κ^2-4,4′-(*n*-nonyl)$_2$-2,2′-bipyridyl ligands.[9] The $^{13}C\{^1H\}$ NMR spectra additionally displayed singlet resonances for the CO carbon nuclei, showing little variation from one complex to next (δ av 207.0). The C_s molecular symmetry is again reflected in the $^{11}B\{^1H\}$ NMR spectra with all three complexes **3** displaying four peaks with an integrated intensity ratio 1:3:2:3, the second and fourth of these likely due to overlap of broad unresolved 1:2 resonances. The chemical shift range for these signals (δ av 0.8 to −18.2) is typical for *closo*-3,1,2-$MC_2B_9H_{11}$ systems,[10] and all resonances showed couplings $^1J_{HB}$ > 100 Hz in the fully coupled ^{11}B NMR spectra, indicating all terminal B−H protons remain intact.

Single crystals of complex **3a** were grown from CH_2Cl_2/hexanes and an X-ray structure determination carried out, the results of which are shown in Figure 1. The basic complex architecture is that of the classic three-legged piano stool motif. Despite the presence of the strong 2,2′-bipyridyl donor, the metal center is fully engaged with the CCBBB coordinating face of the cage in a pentahapto fashion (C(1)−C(2) 1.641(5) Å, Ru−C_{cage} av 2.199 Å, and Ru−B av 2.254 Å), with no evidence of cage slippage or distortion. For comparison, the same bond distances from the structural analysis of compound **2b** gives C(1)−C(2) 1.657(6) Å, Ru−C_{cage} av 2.253 Å, and Ru−B av 2.270 Å. The lone carbonyl ligand of complex **3a** is also bound in the expected linear fashion (Ru(3)−C(3) 1.866(4) Å, C(3)−O(3) 1.154(4) Å, Ru(3)−C(3)−O(3) 175.3(4)°), in addition to the fully chelating, planar 2,2′-bipyridyl ligand (Ru(3)−N(1) 2.093(3) Å, Ru(3)−N(2) 2.135(3) Å, torsion angle N(1)−C(14)−C(15)−N(2) −1.7(5)°). There are no unusual long-range features

(9) Grant, G. J.; Patel, K. N.; Helm, M. L.; Mehne, L. F.; Klinger, D. W.; VanDerveer, D. G. *Polyhedron* **2004**, *23*, 1361.

(10) (a) Heřmánek, S. *Chem. Rev.* **1992**, *92*, 325. (b) Brew, S. A.; Stone, F. G. A. *Adv. Organomet. Chem.* **1993**, *35*, 135.

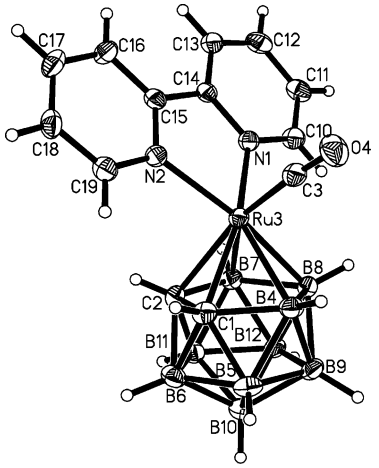

Figure 1. Molecular structure of complex **3a** (thermal ellipsoids with 50% probability). Selected distances (Å) and angles (deg): Ru(3)−C(3) 1.866(4), Ru(3)−N(1) 2.093(3), Ru(3)−N(2) 2.135(3), Ru(3)−C(1) 2.174(4), Ru(3)−C(2) 2.224(4), Ru(3)−B(4) 2.206(5), Ru(3)−B(7) 2.279(4), Ru(3)−B(8) 2.277(4), C(3)−O(4) 1.154(5), C(1)−C(2) 1.641(5); Ru(3)−C(3)−O(4) 175.3(4), C(3)−Ru(3)−N(1) 90.12(15), C(3)−Ru(3)−N(2) 92.04(14), N(1)−Ru(3)−N(2) 76.25(12), N(1)−Ru(3)−C(1) 160.40(13), C(3)−Ru(3)−B(4) 82.18(17), N(2)−Ru(3)−B(4) 140.17(15), C(2)−Ru(3)−C(3) 153.16(16), N(2)−Ru(3)−C(2) 92.17(13), C(1)−Ru(3)−C(2) 43.80(14), N(2)−Ru(3)−B(8) 165.20(13), N(1)−Ru(3)−B(7) 88.04(14); N(1)−C(14)−C(15)−N(2) −1.7(5).

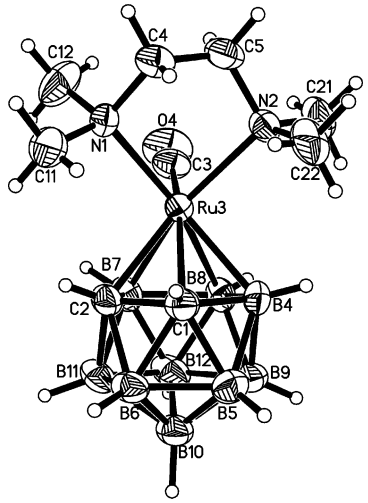

Figure 2. Molecular structure of complex **4** (thermal ellipsoids with 50% probability). Selected distances (Å) and angles (deg): Ru(3)−C(3) 1.840(5), Ru(3)−N(1) 2.270(3), Ru(3)−N(2) 2.232(4), Ru(3)−C(1) 2.224(5), Ru(3)−C(2) 2.190(5), Ru(3)−B(4) 2.207(5), Ru(3)−B(7) 2.242(5), Ru(3)−B(8) 2.251(6), C(3)−O(4) 1.158(5), C(1)−C(2) 1.628(8); Ru(3)−C(3)−O(4) 169.5(5), C(3)−Ru(3)−N(1) 91.66(18), C(3)−Ru(3)−N(2) 91.44(18), N(1)−Ru(3)−N(2) 79.53(15), N(1)−Ru(3)−C(1) 104.74(17), C(3)−Ru(3)−B(4) 123.0(2), N(2)−Ru(3)−B(4) 89.94(16), C(2)−Ru(3)−C(3) 121.2(2), N(2)−Ru(3)−C(2) 147.05(17), C(1)−Ru(3)−C(2) 43.3(2), N(2)−Ru(3)−B(8) 114.78(18), N(1)−Ru(3)−B(7) 117.5(2); N(1)−C(4)−C(5)−N(2) −59.9(6).

regarding the packing of the complex molecules (monoclinic space group $P2_1/n$), such as short intermolecular contacts or π-stacking.

To serve as an aliphatic contrast, TMEDA (*N*,*N*,*N*′,*N*′-tetramethylethylenediamine) was employed as the chelating ligand. The synthesis of [3-CO-3,3-{κ^2-$Me_2N(CH_2)_2NMe_2$}-*closo*-3,1,2-$RuC_2B_9H_{11}$] (**4**) was similar to that of the complexes **3**, with workup yielding vibrant orange microcrystals following chromatography on silica gel and recrystallization from CH_2Cl_2/hexanes. In response to the stronger tertiary trialkylamine donor nature of the ligand, the ν_{max}(CO) absorption for complex **4** is displaced to considerably lower energy (1942 cm^{-1}). Diagnostic signals were also identified in the ^1H NMR spectrum, with the cage C−H protons resonating at δ 3.52, and peaks for the TMEDA ligand at δ 3.01, 2.85 (CH_2), 2.96, and 2.66 (NMe_2). These reflect pseudo-C_s molecular symmetry in solution, no doubt owing to the flexibility of the ethylene chain in the TMEDA ligand. The $^{13}C\{^1H\}$ NMR spectrum of complex **4** also displayed the requisite number of resonances for the TMEDA and cage ligands in addition to a singlet peak at δ 201.8 for the carbonyl carbon nucleus. Finally, the $^{11}B\{^1H\}$ NMR spectrum of complex **4** displayed the full complement of six peaks between the chemical shift limits of δ −0.3 and −22.8 (the accepted *closo*-3,1,2-MC_2B_9 range[10]) with an integrated intensity ratio of 1:1:2:2:2:1. All peaks were fully doublet-coupled ($^1J_{HB}$ > 100 Hz) in a ^{11}B NMR spectrum. It is important to stress at this juncture that routine spectroscopic analysis revealed absolutely no other products or isomers present with any of the complexes **3** or **4** and that purity is further confirmed by elemental analysis (Table 1) for all the compounds reported.

From a crop of crystals of complex **4** grown from CH_2Cl_2/hexanes, it was apparent that two distinct morphologies were presented. Single crystals of the more tractable variety were selected, and a structure determination carried out, the results of which are shown in Figure 2. The structure determination was important for the verification of the monomeric nature of the complex and the role of the TMEDA ligand in particular, given the possibility for this ligand to bridge between distinct metallacarborane moieties.[11] Indeed, the similarities between the structure of this complex and that of complex **3a** described above are tangible, which is surprising because the TMEDA ligand is potentially a much more powerful donor than its planar 2,2′-bipyridyl relative. Of course, it is still a tertiary amine, which may sterically limit its σ-binding ability. Thus, the η^5 binding of the CCBBB cage face with the metal in complex **4** (C(1)−C(2) 1.628(8) Å, Ru−C_{cage} av 2.207 Å, and Ru−B av 2.233 Å) is very similar to that in complex **3a**, with no evidence of cage slippage or distortion between the carbon vertexes. Some caution is required with direct comparison of structural parameters, as the temperatures of the data collections were different (170 (**3a**), 293 K (**4**)), an ambient temperature measurement being required for complex **4** because of problems encountered with datasets acquired at the lower temperature, possibly due to interference from a proximal phase transition. Nevertheless, the slightly more potent σ-donation of the TMEDA ligand is reflected, albeit subtly, in the metal−carbonyl bonding distances with a shorter Ru(3)−C(3) distance (1.840(5) Å (**4**) vs 1.866(4) Å (**3a**)) although with statistically the same C(3)−O(4) bond lengths (1.158(5) Å (**4**) vs 1.154(4) Å (**3a**)). The CO ligand itself remains essentially linearly bound (Ru(3)−C(3)−O(4)

(11) Ellis, D. D.; Jeffery, J. C.; Jelliss, P. A.; Kautz, J. A.; Stone, F. G. A. *Inorg. Chem.* **2001**, *40*, 2041.

Table 3. Electrochemical Measurements[a]

A

	MeCN								CH_2Cl_2	
	0/−				**−/2−**				**0/−**	
	$E_{1/2}$/V	ΔE_p/mV[b]	ΔE_{pc}/mV[c]	i_{pa}/i_{pc}[d]	$E_{1/2}$/V	ΔE_p/mV[b]	ΔE_{pc}/mV[c]	i_{pa}/i_{pc}[d]	$E_{1/2}$/V	i_{pa}/i_{pc}[d]
3a	−1.78	73	6	0.96, 0.94	−2.26	105[e]	21	0.45, 0.50	−1.75	0.70, 0.91
3b	−1.82	77	8	0.94, 0.87	−2.29	125	23	0.35, 0.45	−1.82	0.66, 0.72
3c	−1.86	77	2	0.91, 0.95	−2.28	140	37	0.55, 0.46	−1.84	0.42, 0.94
4	−1.94[f,g]	−	45	−					−1.96[f]	−

B

	MeCN									CH_2Cl_2	
	+/0				**+/0**[h]					**+/0**	
	$E_{1/2}$/V	ΔE_p/mV[b]	ΔE_{pa}/mV[c]	i_{pa}/i_{pcd}[d]	$E'_{1/2}$/V	$\Delta E'_p$/mV[b]	$\Delta E'_{pa}$/mV[c]	i'_{pa}/i'_{pc}[d]	i_{pa}/i'_{pc}[i]	$E_{1/2}$/V	i_{pa}/i_{pc}[d]
3a	0.87[j]	−	38	−	0.15	51	10	0.31, 0.82	11.61, 2.61	0.96	−,[k] 1.72
3b	0.85[j]	−	42	−	0.12	48	11	0.27, 0.80	8.48, 2.33	0.93	−,[k] 1.70
3c	0.84[j]	−	43	−	0.11	54	10	0.40, 0.75	4.97, 2.78	0.92	−,[k] 1.57
4	0.75	75	15	1.36, 1.11						0.83	1.05, 1.02

[a] Measured at 298 K on 1.00 mM (MeCN or CH_2Cl_2) solutions of the complexes. Charges shown (in bold) represent overall complex charge. [b] Peak separation at slow scan rates (0.05 V s^{-1}). [c] Peak shift in mV decade^{-1} increase in scan rate. [d] Anodic to cathodic peak current ratio at scan rate 0.05 V s^{-1}. For quasi-reversible couples, ratios are quoted for scan rates 0.05, 1.00 V s^{-1}, respectively. [e] ΔE_p = 118 mV at scan rate 0.10 V s^{-1} (used in simulation). [f] E_{pc} value reported for irreversible reduction. [g] Followed by a weaker, irreversible wave with E_{pc} = −2.15 V. [h] Not observed without prior initial oxidation of complexes **3**. Attributed to redox couple for MeCN adducts, **3′** (see text). [i] Ratio of the anodic peak for the parent complex **3** to the cathodic peak for the MeCN adduct **3′**. [j] E_{pa} value reported for irreversible oxidation. [k] Irreversible at low scan rates.

169.5(5)°). The ruthenium−nitrogen bond lengths (Ru(3)−N(1) 2.270(3) Å, Ru(3)−N(2) 2.232(4) Å) are somewhat longer than the corresponding distances in complex **3a**, as might be expected with tertiary amino sp^3-hybridized *N*-donor atoms, in addition to being unequal, Δd = 0.038 Å. These distances are also notably longer than those of the 16-electron cyclopentadienide complexes [Ru(η^5-C_5R_5){κ^2-$Me_2N(CH_2)_2NMe_2$}][B{$C_6H_3(CF_3)_2$-3,5}$_4$] (R = H,[12] Me[13]), which have Ru−N bond lengths of 2.142(6) Å, 2.163(8) Å (R = H) and 2.183(7) Å, 2.180(6) Å (R = Me), respectively. The Ru−N distances of complex **4** compare more favorably, however, with those of the 18-electron complex [Ru(η^6-C_5H_4-CH_2){κ^2-$Me_2N(CH_2)_2NMe_2$}(OH)][B{$C_6H_3(CF_3)_2$-3,5}$_4$](Ru−N 2.213(5) Å, 2.238(5) Å).[13]

Electrochemistry and Spectroelectrochemistry. Cyclic voltammetry (CV) data for complexes **3** and **4** are reported in Table 3. Measurements for the complexes **3** in the reductive-cathodic regime (Table 3A, Figure 3) reveal a reversible one-electron reduction with an expected correlation of $E_{1/2}$ values in MeCN with bipyridyl ring-donor potency: $E_{1/2}$ = −1.78 V (R = H, **3a**), −1.82 V (R = $(CH_2)_8Me$, **3b**), −1.86 V (R = Bu^t, **3c**). For all three complexes, this first redox process is diffusion controlled in both directions, exemplified by linear $|i_p| - \nu^{1/2}$ plots for complex **3a** in Figure 4. Similar data are observed in CH_2Cl_2, but are quasi-reversible, with the anions generated not surprisingly being less stable in this solvent. In MeCN, peak separations (ΔE_p) and displacement of cathodic peaks with scan rate (ΔE_{pc}) are consistent with moderately fast electron transfer followed by no appreciable chemical reaction. While it is tempting to target the 2,2′-bipyridyl ring as the site of reduction to yield

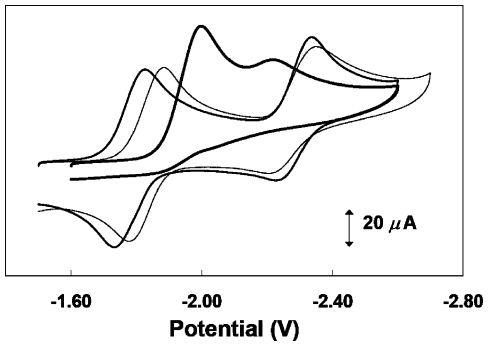

Figure 3. Reductive-cathodic cyclic volatmmograms (scan rate 1.00 V s^{-1}) for MeCN (1.0 mM) solutions of complexes **3a** (medium line), **3c** (thin line), and **4** (thick line).

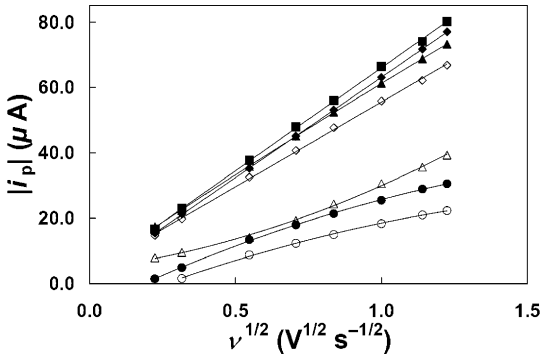

Figure 4. Diffusion control $|i_p| - \nu^{1/2}$ plots for complex **3a** from cyclic voltammograms measured in MeCN: ◆/◇ (**3a**/**3a**$^-$), ▲/△ (**3a**$^-$/**3a**$^{2-}$), ■ (**3a**$^+$/**3a**), ●/○ (**3a′**$^+$/**3a′**).

(bipy$^-$)Ru^{II}(cage), a more likely scenario is the formation of (bipy)Ru^I(cage) for two reasons: (i) Deronzier, Ziessel, and Pakkanen et al. have reported that 2-electron reduction of [Ru(*trans*-Cl)$_2${κ^2-2,2′-$(NC_5H_4)_2$}$(CO)_2$] at $E_{1/2}$ = −1.78 V in MeCN yields a Ru^I metal center (with concomitant Cl$^-$ loss), which subsequently undergoes dimerization;[14] (ii) our own spectroscopic measurements (vide infra) support a

(12) Gemel, C.; Huffman, J. C.; Caulton, K. G.; Mauthner, K.; Kirchner, K. *J. Organomet. Chem.* **2000**, *593*−*594*, 342.
(13) Gemel, C.; Mereiter, K.; Schmid, R.; Kirchner, K. *Organometallics* **1997**, *16*, 5601.

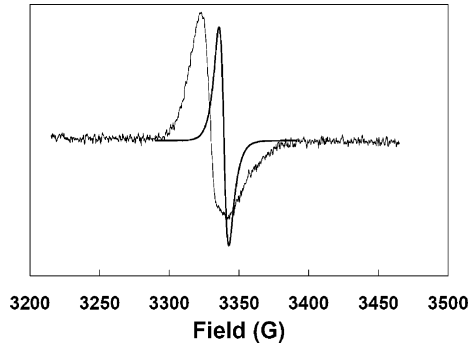

Figure 5. X-band EPR spectra (298 K) of complex **3c** following reduction with 1 mol equiv of $NaC_{10}H_8$: THF (94 mM) solution (thick line), $g_{iso} = 1.9972$; microcrystalline solid sample (thin line), $g_{1,2} = 1.9995$, $g_3 = 1.9925$.

metal-centered LUMO (lowest unoccupied molecular orbital), rather than a 2,2′-bipyridyl-based empty π^* orbital as the LUMO in the complexes **3**.

Treatment of complex **3c** with 1 mol equiv of $NaC_{10}H_8$ (sodium naphthalenide) in THF gave a wine red solution, which was extremely air-sensitive and was not subjected to isolation procedures. However, an in situ EPR spectrum of complex $\mathbf{3c}^-$ in THF (Figure 5) displayed a highly isotropic signal ($g_{iso} = 1.9972$). A solid sample, produced by removal of THF in vacuo and pumping for ca. 2 h, produced an EPR envelope with only a slightly higher degree of anisotropy in the g-tensor ($g_{1,2} = 1.9995$, $g_3 = 1.9925$). The resonance is also broader, which could be attributed to the influence of the carborane ^{11}B nuclei (spin 3/2). This is reminiscent of the reported EPR analysis of the 17-electron paramagnetic complex, $[N(PPh_3)_2][1,1,1\text{-}(CO)_3\text{-}2\text{-}Ph\text{-}isocloso\text{-}1,2\text{-}MnCB_9H_9]$,[15] and lower anisotropy associated with small Δg values has been previously reported for a number of smaller paramagnetic metallacarboranes with odd PSE (polyhedral skeletal electron) counts (<18-electron metal complexes) and low symmetry.[16] If nothing else, the EPR measurement serves to verify that the unpaired electron in $\mathbf{3c}^-$ is not confined to the 2,2′-bipyridyl ligand, as might be expected in complexes comprising the $[RuL_{6-2n}(2,2'\text{-bipyridyl})_n]^+$ (L = neutral 2-electron donor, $n = 1-3$) unit. Such classical paramagnetic 2,2′-bipyridyl ruthenium complexes display discernible nitrogen hyperfine splitting, even in solution at ambient temperatures, providing inter-ring electron transfer between multiple 2,2′-bipyridyl rings has been quenched.[17] This in turn supports the notion of a metal d* SUMO (singly occupied molecular orbital), but with significant delocalization onto the carborane ligand.

A second, quasi-reversible one-electron reduction was observed in MeCN for all complexes **3**, ($-2.26 < E_{1/2} < -2.29$ V) that was not observed within the CH_2Cl_2 solvent window. A departure from diffusion control for this second reduction for complex **3a** (representative of all three complexes **3**) is subtle at best, with deviation from linearity in the $|i_p| - \nu^{1/2}$ plot (Figure 4) being more perceptible for the reoxidation of the dianion, $\mathbf{3a}^{2-}$. At a scan rate of 0.10 V s^{-1}, the peak separation $\Delta E_p = 116$ mV, which compared with the first reduction ($\Delta E_p = 78$ mV at the same scan rate), certainly suggests slower heterogeneous electron-transfer kinetics. Analysis by the Nicholson method[18] gives a kinetic parameter, $\Psi = 0.394$, and from chronoamperometric analysis of complex **3a** (1.00 mM solution in MeCN), the diffusion coefficient for the singly reduced monoanion $\mathbf{3a}^-$ was calculated, $D_{\mathbf{3a}^-} = 1.3 \times 10^{-5}$ cm^2 s^{-1}. These parameters combined to give a reasonable estimate for the heterogeneous electron-transfer rate constant, $k_{ET} = 0.016$ cm s^{-1} at 298 K. There has been only one notable study of the kinetic parameters involving electron transfer with metallacarboranes.[19,20] In particular, sandwich complexes of the type $[3,3'\text{-M-}(closo\text{-}1,2\text{-}C_2B_9H_{11})_2]^{x-/(x+1)-}$ (M = Co, Ni; $x = 0$, 1) have been determined to undergo reasonably rapid heterogeneous electron transfer ($k_{ET} = 0.14-250$ cm s^{-1}) at a MeCN/Hg interface, with minor molecular conformational changes or solvent reorganization being invoked to account for low activation energy barriers associated with these redox events. These values are more than an order of magnitude greater than that observed for complex **3a** in the same solvent, supporting the notion of some structural modification. For comparative purposes, the difference in working electrodes (mercury vs glassy carbon in our experiments) is not expected to significantly impact k_{ET} values for outer-sphere electron transfer, given there are no apparent adsorption effects operating.[21] In the current work, this assertion is supported by CV measurements of the complexes **3** in MeCN using an Au disk working electrode, which showed little difference (ca. 10−20 mV) in peak separations, ΔE_p, compared with the glassy carbon working electrode used for the data presented in Table 3. A simulated CV for complex **3a** is given in the Supporting Information, Figure S1. As can be seen, the matching between real and simulated voltammograms is hampered by the proximity of the second reduction potential to the solvent window. Nevertheless, the general form and ΔE_p value are reasonably digitally reproduced by employment of diffusion coefficients, ($D_{\mathbf{3a}^-} = 1.3 \times 10^{-5}$ cm^2 s^{-1}, $D_{\mathbf{3a}^{2-}} = 2.4 \times 10^{-6}$ cm^2 s^{-1} from chronoamperometric measurements), transfer coefficient, $\alpha = 0.5$, and a moderately slow electron-transfer rate for $\mathbf{3a}^-/\mathbf{3a}^{2-}$, $k_{ET} = 0.02$ cm s^{-1}. The best match was obtained on the basis of an $\vec{\mathbf{E}}C$ mechanism, using values of $K_{eq} = 10$, $k_f = 100$ s^{-1} for the homogeneous reaction. Adjustments of the mechanism and parameters verified that any structural

(14) Chardon-Noblat, S.; Deronzier, A.; Zsoldos, D.; Ziessel, R.; Haukka, M.; Pakkanen, T.; Venäläinen, T. *J. Chem. Soc., Dalton Trans.* **1996**, 2581.
(15) Du, S.; Farley, R. D.; Harvey, J. N.; Jeffery, J. C.; Kautz, J. A.; Maher, J. P.; McGrath, T. D.; Murphy, D. M.; Riis-Johannessen, T.; Stone, F. G. A. *J. Chem. Soc., Chem. Commun.* **2003**, 1846.
(16) Tomlinson, S.; Zheng, C.; Hosmane, N. S.; Yang, J.; Wang, Y.; Zhang, H.; Gray, T. G.; Demissie, T.; Maguire, J. A.; Baumann, F.; Klein, A.; Sarkar, B.; Kaim, W.; Lipscomb, W. N. *Organometallics* **2005**, *24*, 2177.
(17) (a) DeArmond, M. K.; Tait, D. D.; Gex, J.-N.; Wertz, D. W.; Hanck, K. W.; Kaneko, M. *J. Phys. Chem.* **1989**, *93*, 977. (b) Gex, J.-N.; Brewer, W.; Bergmann, K.; Tait, C. D.; DeArmond, M. K.; Hanck, K. W.; Wertz, D. W. *J. Phys. Chem.* **1987**, *91*, 4776. (c) Gex, J.-N.; DeArmond, M. K.; Hanck, K. W. *J. Phys. Chem.* **1987**, *91*, 251.
(18) Nicholson, R. S. *Anal. Chem.* **1965**, *37*, 667.
(19) Geiger, W. E., Jr.; Smith, D. E. *J. Electroanal. Chem.* **1974**, *50*, 31.
(20) Morris, J. H.; Gysling, H. J.; Reed, D. *Chem. Rev.* **1985**, *85*, 51.
(21) (a) Mukherjee, R. N.; Pulla Rao, Ch.; Holm, R. H. *Inorg. Chem.* **1986**, *25*, 2979. (b) Bowyer, W. J.; Geiger, W. E. *J. Am. Chem. Soc.* **1983**, *105*, 1903. (c) Sharp, P. R.; Bard, A. J. *Inorg. Chem.* **1983**, *22*, 3462.

Chart 2. Options for Structural Rearrangement upon Addition of a Second Electron to the Complexes **3**[a]

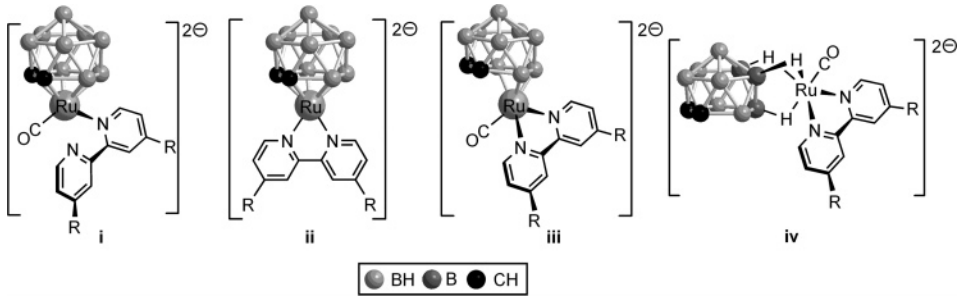

[a] (i) $\kappa^2 \rightarrow \kappa^1$ partial displacement of the 2,2′-bipyridyl ligand; (ii) CO dissociation; (iii) $\eta^5 \rightarrow \eta^3$ haptotropic cage ligand slippage; (iv) *closo* → *exonido* dislocation.

transformation is not likely to be occurring before the second reduction or that the heterogeneous electron transfer can be much faster, as with previous metallacarborane examples. Indeed, further refinement of the K and k_f values necessitated a substantial decrease in k_{ET} to achieve anything near the fit displayed in Figure S1.

Solvation alone is unlikely to account for such slow electron transfer, which is evident of a more severe inner sphere reorganization. Capture of the second electron could precipitate the partial dislocation of the 2,2′-bipyridyl ligand (i), CO dissociation (ii), $\eta^5 \rightarrow \eta^3$ cage slippage (iii), or *closo* → *exonido* transformation (iv) as depicted in Chart 2. While the first and second of these (effectively d^{10} ML_2 vertexes) are not uncommon or unexpected, the third has precedent in early work on the redox behavior of [3,3′-Ni-(*closo*-1,2-$C_2B_9H_{11})_2]^{x-/(x+1)-}$ ($x = 0$, 1)[19,22] and manifests itself in the X-ray structure determination of the complex [3-H-3,3-$(PPh_3)_2$-3,8-μ-{$Au(PPh_3)$}-η^3-$IrC_2B_9H_{10}$].[23] Both the fully reduced Ni^{II} species and the $Ir^{III}Au$ complex comprise slipped η^3 carborane cage ligands, the consequence of an $\eta^5 \rightarrow \eta^3$ shift being a switch from the usual 4-electron to 2-electron donation, i.e., cage slippage relieves electron density build-up at the metal center, and such a structural alteration in $\mathbf{3}^{2-}$ to give outcome (iii) is entirely feasible. Outcome (iv) involves the dislocation of the metal fragment to the exterior of the cage, yielding an *exonido* species. However, although there are a number of characterized Ru^{II} species involving *exonido* dianionic dicarbollide ligands,[24] the formation of B−H→Ru agostic bonds between a highly charged carborane cage and a formally zero-valent Ru^0 center is thought unlikely. It should be disclosed that the same measurement

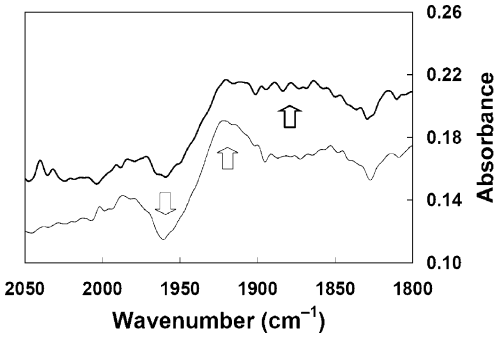

Figure 6. Difference CA-IR spectra for the reduction of a solution of complex **3c** in MeCN (1.0 mM): potential held at −1.70 V (thin line); −2.30 V (thick line).

in THF produced a cyclic voltammogram very similar in appearance, but with the second reduction at a more negative potential ($E_{1/2} = -2.55$ V for complex **3a**) and inflated peak separations due to expected resistance effects.

Spectroelectrochemical analysis of the reduction of complex **3c** in MeCN was attempted, the results of which are shown in Figure 6. While solvents most suitable for reduction (MeCN, THF) are less than ideal for this technique, measurement while holding the potential at −1.70 V to capture the first reduction did show the consumption of the neutral complex **3c** (ν_{max}(CO) = 1960 cm^{-1}) and appearance of a new absorption at 1920 cm^{-1}. The nominal change in resonance frequency, $\Delta\nu$, upon a change in metal oxidation state of ±1 is usually 100−150 cm^{-1},[25] which along with the EPR analysis of complex **3c** following reduction, leads us to presume again that the SOMO in $\mathbf{3c}^-$ (and by inference the LUMO in neutral complex **3c**) is not entirely metal-centered but heavily delocalized about the carborane cage ligand. A further drop in potential to −2.30 V resulted in a broad increase in absorbance in the region around 1880 cm^{-1}, a feature which was consistently observed upon a number of measurements. Because of the likelihood of solvent interference under these conditions, it is impossible to conclude anything further about the structural state of the doubly reduced species $\mathbf{3c}^{2-}$.

Complex **4** also underwent a one-electron reduction, though irreversibly so and at an even lower potential (E_{pc} =

(22) (a) Warren, L. F.; Hawthorne, M. F. *J. Am. Chem. Soc*., **1968**, *90*, 4823; **1970**, *92*, 1157. (b) Wing, R. M. *J. Am. Chem. Soc*. **1968**, *90*, 4828.

(23) Jeffery, J. C.; Jelliss, P. A.; Stone, F. G. A. *J. Chem. Soc., Dalton Trans.* **1993**, 1083.

(24) (a) Chizhevsky, I. T.; Lobanova, I. A.; Bregadze, V. I.; Petrovskii, P. V.; Antonovich, V. A.; Polyakov, A. V.; Yanovskii, A. I.; Struchkov, Y. T. *Mendeleev Commun.* **1991**, 47. (b) Viñas, C.; Nuñez, R.; Flores, M. A.; Teixidor, F.; Kivekäs, R.; Sillanpää, R. *Organometallics* **1995**, *14*, 3925; **1996**, *15*, 3850. (c) Ellis, D. D.; Jelliss, P. A.; Stone, F. G. A. *Organometallics* **1999**, *18*, 4982. (d) Lobanova, I. A.; Bregadze, V. I.; Timofeev, S. V.; Petrovskii, P. V.; Starikova, Z. A.; Dolgushin, F. M. *J. Organomet. Chem*. **2000**, *597*, 48. (e) Timofeev, S. V.; Lobanova, I. A.; Petrovskii, P. V.; Starikova, Z. A.; Bregadze, V. I. *Russ. Chem. Bull*. **2001**, *50*, 2245. (f) Lobanova, I. A.; Khitrova, O. M.; Petrovskii, P. V.; Bregadze, V. I. *Russ. Chem. Bull*. **2004**, *53*, 251. (g) Cheredilin, D. N.; Dolgushin, F. M.; Balagurova, E. V.; Godovikov, I. A.; Chizhevsky, I. T. *Russ. Chem. Bull*. **2004**, *53*, 2086.

(25) (a) Connelly, N. G.; Johnson, G. A. *J. Organomet. Chem*. **1974**, *77*, 341. (b) Carriedo, G. A.; Riera, V.; Connelly, N. G.; Raven, S. J. *J. Chem. Soc., Dalton Trans*. **1987**, 1769.

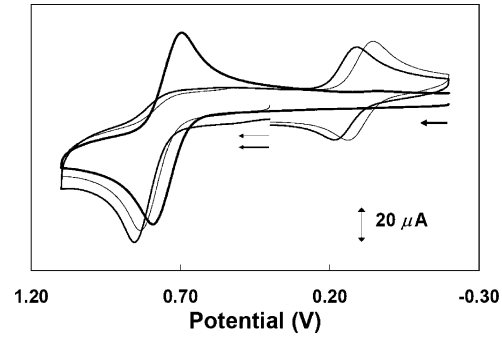

Figure 7. Oxidative-anodic CVs (scan rate 1.00 V s^{-1}) of MeCN (1.0 mM) solutions of complexes **3a** (medium line), **3c** (thin line), and **4** (thick line).

−1.94 V). In MeCN, a further, smaller wave is also noted at −2.15 V (Figure 3).

All four complexes displayed interesting oxidative-anodic electrochemical behavior (Table 3B). Complexes **3** underwent quasi-reversible oxidations in CH_2Cl_2 ($E_{1/2}$ = 0.96 V (**3a**), 0.93 V (**3b**), 0.92 V (**3c**)) with ease of oxidation inversely correlating with strength of donor substituent (H, $(CH_2)_8Me$, Bu^t) on the 2,2′-bipyridyl ligand. For complex **3a** in particular, oxidation is essentially irreversible at low scan rates as seen in the Supporting Information, Figure S2. It was discovered that, curiously, the oxidation of complexes **3** in MeCN appeared to be irreversible at all scan rates but with E_{pc} values lower than in CH_2Cl_2 (E_{pc} = 0.87 V (**3a**), 0.85 V (**3b**), 0.84 V (**3c**)), as might be expected with the more polar solvent. Analysis of anodic peak displacement with scan rate (ΔE_{pa} = 38−43 mV $decade^{-1}$ increase in scan rate) was suggestive of an $\vec{\mathbf{E}}C$ mechanism with a rapid irreversible chemical reaction following electron transfer. More careful scrutiny using a wider scan range, however, revealed a new redox couple at some 0.75 V lower potential ($E_{1/2}$ = 0.15 V (**3a′**), 0.11 V (**3b′**), 0.10 V (**3c′**)) (Figure 7), and it was established that this new redox event was not observed without prior oxidation at higher potential in all cases. The initial oxidation was essentially diffusion controlled, again demonstrated for complex **3a** (Figure 4) as typical for all three complexes **3**. The subsequent **3a′**$^+$/**3a′** couple shows some nonlinearity in its $|i_p| - \nu^{1/2}$ plot, with currents at low scan rates diminished by probable instability of the initial oxidation product **3a**$^+$. This second couple behaved as a simple, rapid $\vec{\mathbf{E}}$ process for all complexes **3** with peak separations close to ΔE_p = 59 mV and little variation of anodic/cathodic peak potentials with scan rate. Reversibility is clearly a function of scan rate, with substantial deterioration of both peaks below 1.00 V s^{-1} (i'_{pa}/i'_{pc} = 0.27−0.40), again no doubt a consequence of the instability of the oxidized species, **3**$^+$, and the wide potential gap between the two redox processes. At 1.00 V s^{-1}, the relationship of initial anodic peak current to the cathodic peak current (i_{pa}/i'_{pc}) for the chemically altered species lies in the range 2.33−2.78. A digitally simulated $\vec{\mathbf{E}}C\vec{\mathbf{E}}$ plot for complex **3c** (the subject of spectroelectrochemical analysis, vide infra) reflected this fairly well (Supporting Information, Figure S3), although adequately modeling the capacitance was problematic. Nevertheless, with diffusion coefficients taken in part from chronoamperometric measurements ($D_{\mathbf{3c}}$ = 2.2 × 10^{-5} cm^2 s^{-1}, $D_{\mathbf{3c}^+}$ = 8.0 × 10^{-6} cm^2 s^{-1} (estimated), $D_{\mathbf{3c}'^+}$ = 8.3 × 10^{-6} cm^2 s^{-1}, $D_{\mathbf{3c}'}$ = 2.0 × 10^{-5} cm^2 s^{-1}(estimated)), peak positions were reproduced with E_{pa} = 0.84 for **3c**$^+$/**3c** (based on a modeled value of $E_{1/2}$ = 0.81 V) and $E_{1/2}$ = 0.11 V for the chemically modified **3c′**$^+$/**3c′** pair. Although the latter redox process was essentially symmetric (α = 0.5), it was necessary to introduce some asymmetry into the initial oxidation (α = 0.45) and both processes appear to proceed with moderately slow homogeneous electron-transfer rates (k_{ET} = 0.02 (**3c**$^+$/**3c**) and 0.03 cm s^{-1} (**3c′**$^+$/**3c′**)), which seems to be in line with that observed in the reductive processes accompanied by structural transformation (vide supra). The chemical reaction was best modeled with K_{eq} = 50 and k_f = 250 s^{-1}. The simulation also correctly predicted a diminished peak current, i_{pa}, upon the second cycle, which was observed in the experiment (Figure S3).

Measured under similar conditions, complex **4**, however, displayed a simple reversible one-electron oxidation in both MeCN ($E_{1/2}$ = 0.75 V, Figure 7) and CH_2Cl_2 ($E_{1/2}$ = 0.83 V, Figure S2), with no associated additional redox couple observed at any scan rate or concentration, even with continuous cycling (5 h at 0.10 V s^{-1}). Diffusion control was evident from measurements in both scanning directions. In MeCN, the oxidative **4**$^+$/**4** redox couple appears to be fully reversible at scan rates above 1.00 V s^{-1} but is better described as quasi-reversible at <0.10 V s^{-1}. In CH_2Cl_2, however, the couple is fully reversible at all scan rates. Little variation of peak potential (ΔE_{pa} = 15 mV) with scan rate in MeCN implies a simple $\vec{\mathbf{E}}$ process with somewhat sluggish heterogeneous electron transfer (ΔE_p = 75 mV). Digital simulation of the MeCN voltammogram at a scan rate of 1.00 V s^{-1} suggests an $\vec{\mathbf{E}}C$ mechanism may be more accurate, though with a reactant(**4**$^+$)-favored homogeneous chemical reaction (K_{eq} = 0.4) following moderately slow heterogeneous electron transfer (k_{ET} = 0.03 cm s^{-1}), though apparently not quite slow enough to remove the system from a diffusion-controlled regime. While solvation of the cationic complex by MeCN may play a role, a more structurally perturbationary event is conceivable and will be discussed further momentarily. Chronoamperometric Cottrell plots for the oxidations of both **3c** and **4** are shown in the Supporting Information, Figure S4. The extracted data for complex **4** ($D_{\mathbf{4}}$ = 4.4 × 10^{-5} cm^2 s^{-1}, $D_{\mathbf{4}^+}$ = 1.1 × 10^{-5} cm^2 s^{-1}) were used in the simulation seen in the Supporting Information, Figure S5. Although the data for the two systems are plotted with slightly different abscissa in Figure S4, it can be seen that the decrease in diffusion coefficient of the cationic oxidized species (**3c**$^+$,**4**$^+$) relative to the parent neutral complex (**3c**,**4**) is approximately the same (ca. 30%) for both complexes. Thus, one option for complex **3c** in particular, namely that of dimerization of the 17-electron ruthenium centers, can be ruled out, and in both cases monomeric products are prevalent.

The starting materials **3** and **4** comprise a d^8 ML_3 vertex, which contributes one PSEP (polyhedral skeletal electron pair) to cage-cluster counting,[26] ultimately giving a 13 (n+1)

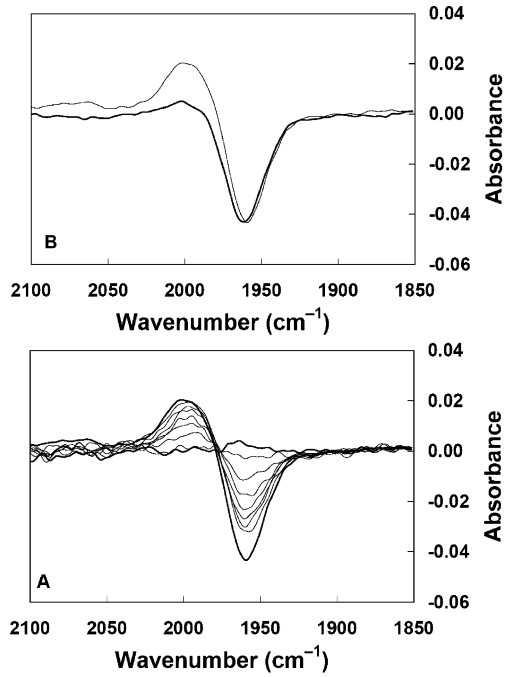

Figure 8. Difference CV−IR spectra for the oxidation of a 1.0 mM solution of complex **3c** in CH_2Cl_2. (**A**) Sampled over the first minute of potential cycling (0.7−1.3 V, 0.80 V s^{-1}). (**B**) Measurements at the end of the data collection: neat CH_2Cl_2 solution (thin line); +30 μL MeCN (thick line).

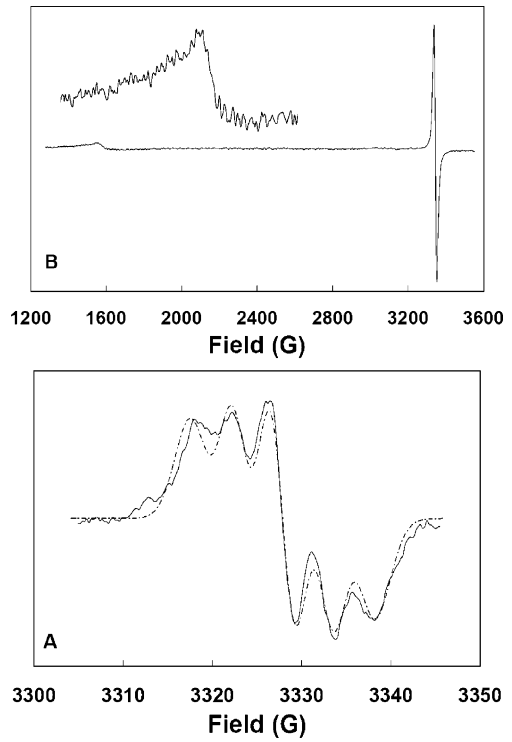

Figure 9. X-band EPR spectra (298 K) of complex **4** following oxidation with 0.9 mol equiv of $[N(C_6H_5Br\text{-}4)_3][SbCl_6]$. (**A**) Sample in CH_2Cl_2 (26 mM) solution: (thin line) measured spectrum; (hashed line) simulated spectrum, g_{iso} = 2.0031, A_N = 0.45 mT, line width = 0.40 mT. (**B**) Microcrystalline solid sample, g_1 = 4.2940, $g_{2,3}$ = 1.9920. Inset shows expansion of g_1 tensor.

PSEP *closo* icosahedron. From the perspective of metallacarborane cluster chemistry, some structural modification of both complexes **3** and **4** upon oxidation is feasible on the basis of the observed electrochemical data. Einholz and coworkers have described the electrochemical formation of $[hypercloso\text{-}B_{10}X_{10}]^-$ (X = Cl, Br) following one-electron oxidation of $[closo\text{-}B_{10}X_{10}]^{2-}$.[27] This was at variance with the nonhalogenated congeners $[closo\text{-}B_nH_n]^{2-}$ (n = 10, 12), which have been observed to undergo dimerization upon electrochemical oxidation, affording $[conjuncto\text{-}B_{2n}H_{2n-1}]^{3-}$ moieties.[28] Although the occurrence of *hypercloso* or *isocloso*[29] metallaborane and metallacarborane is uncommon, it is well documented for species with n PSEP (n = number of vertexes) and a number of complexes have been structurally characterized.[30] In particular, *isocloso*-MC_2B_9 clusters are seen to adopt a formally η^6-C_2B_4 cage ligation versus the more typical η^5-C_2B_3 coordination in regular $n + 1$ *closo* icosahedral-based metallacarborane systems.[31] As yet, however, there have been no reports of $n + 0.5$ PSEP *isocloso* 12-vertex metallacarboranes, although Stone et al. have recently described the synthesis and characterization of the aforementioned 11-vertex *isocloso* monocarbollide species $[N(PPh_3)_2][1,1,1\text{-}(CO)_3\text{-}2\text{-}Ph\text{-}isocloso\text{-}1,2\text{-}MnCB_9H_9]$.[15] We also note that there is a remarkable paucity of cationic metallacarboranes in the literature. In an attempt to further probe the oxidized species $\mathbf{3c}^+$ and $\mathbf{4}^+$, therefore, spectroelectrochemical CV−IR analysis was performed. For a 1.0 mM solution (10 mL) of complex **3c** in CH_2Cl_2, continuously cycling the potential between 0.7 and 1.3 V at a scan rate of 0.8 V s^{-1} yielded the series of difference IR spectra shown in Figure 8A. The disappearance of the neutral complex **3c** (ν_{max}(CO) = 1961 cm^{-1}) is apparent, while the growth of a new vibrational resonance at ν_{max}(CO) = 1998 cm^{-1} is striking, albeit at a diminished rate. This latter observation is perhaps to be expected, given the lack of reversibility of this couple for **3c** (and all complexes **3**) in CH_2Cl_2 at lower

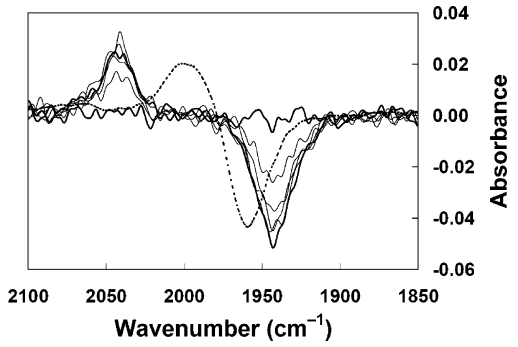

Figure 10. Difference CV−IR spectra for the oxidation of a 1.0 mM solution of complex **4** in CH_2Cl_2 with the potential cycled between 0.8 and 1.3 V (0.8 V s^{-1}). For comparative purposes, the final measurement for the spectroelectrochemically observed oxidation of **3c** is included (hashed line).

(26) O'Neill, M. E.; Wade, K. In *Comprehensive Organometallic Chemistry*; Wilkinson, G., Abel, E. W., Stone, F. G. A., Eds.; Pergamon Press: Oxford, 1982; Vol. 1, Section 1.
(27) Einholz, W.; Vaas, K.; Wieloch, C.; Speiser, B.; Wizemann, T.; Ströbele, M.; Meyer, H.-J. *Z. Anorg. Allg. Chem.* **2002**, *628*, 258.
(28) (a) Middaugh, R. L.; Farha, F., Jr. *J. Am. Chem. Soc.* **1966**, *88*, 4147. (b) Wiersema, R. J.; Middaugh, R. L. *J. Am. Chem. Soc.* **1967**, *89*, 5078.
(29) It has been indicated that under these circumstances closed, deltahedral metallaboranes and metallacarboranes with $< n + 1$ PSEP should be more appropriately referred to as *isocloso* rather than *hypercloso*: Kennedy, J. D. *Inorg. Chem.* **1986**, *25*, 111.

Scheme 1. Substitution Lability upon Electrochemical Oxidation of the Complexes **3** in MeCN

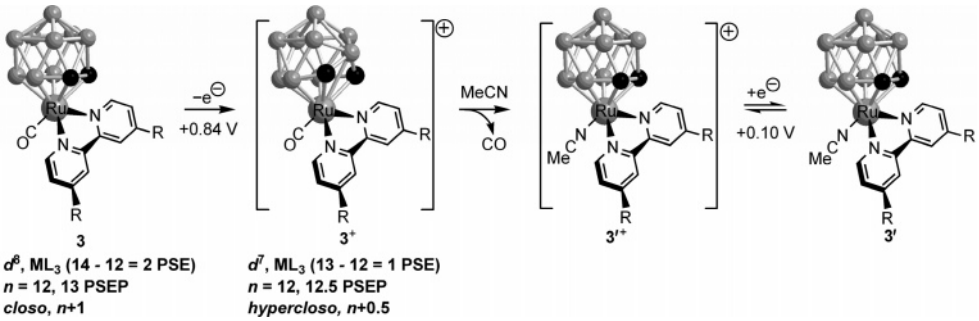

scan rates and some CO loss and decomposition may be occurring. Nevertheless, an increase in carbonyl stretching frequency of $\Delta\nu = +37$ cm^{-1} is substantially below the increase of ca. 100−150 cm^{-1} expected when an organometallic carbonyl complex is oxidized to the tune of one electron (increasing formal oxidation state by +1).[25] In a poorly coordinating solvent such as CH_2Cl_2, a sudden loss of electron density at the metal center could be mitigated by a *closo* → *isocloso* structural transformation, or from a coordination complex-ligand perspective, an $\eta^5 \rightarrow \eta^6$ change in hapticity of the C_2B_9 cage (Scheme 1). This is clearly not the ultimate fate of complex **3c** in MeCN, however. The above-discussed electrochemical data support a rapid ligand substitution in the oxidized complex **3c**$^+$, namely MeCN for CO, to yield **3c′**$^+$, which may be subsequently reduced to **3c′** at ca. 0.75 V lower potential. The substitution of a strong π-acid (CO) for a considerably more powerful donor (MeCN) is a logical consequence to offset the loss of electron density. To test this hypothesis, the same CH_2Cl_2 solution of complex **3c** was treated with 30 μL of MeCN (ca. 60 mol equiv) and the CV−IR spectroelectrochemical scan repeated. As can be seen from Figure 8B, the resonance at 1998 cm^{-1} is significantly diminished in absorbance at the same measurement time and a CV measurement, which previously showed no redox couple in the vicinity of 0.1 V in this solvent, now showed activity in this region.

Attempts to isolate the cationic species **4**$^+$ as its $[SbCl_6]^-$ salt by treatment of complex **4** with the ammoniumyl salt $[N(C_6H_4Br\text{-}4)_3][SbCl_6]$ in CH_2Cl_2 met with partial success: although the salt could not be isolated and structurally characterized, an EPR measurement of a solution of oxidized complex **4** displayed an expected isotropic signal ($g_{iso} = 2.0031$) with significant hyperfine splitting to two equivalent ^{14}N nuclei ($A_N = 0.45$ mT) as verified by simulation (Figure 9A). This is in keeping with a metallacarborane cage that maintains the integrity of the pseudo-mirror plane in solution. A microcrystalline solid sample revealed a resonance with severe axial distortion ($g_1 = 4.2940$, $g_{2,3} = 1.9920$) confirmed by inspection of the integrated spectrum (Figure 9B). The broadness of the signal cloaked any hyperfine splitting. The combined interpretation of the EPR spectra is that the complex **4**$^+$ SOMO is likely a d orbital not engaged with delocalized cage framework MOs but intimately associated with the 2,2′-bipyridyl nitrogen σ-donor orbitals. The axial appearance in the solid-state sample spectrum may be attributed to the free rotation of the Ru(CO)(κ^2-TMEDA) vertex relative to the carborane cage ligand on the EPR time scale. Such a phenomenon has been identified in the EPR spectra of the 17-electron complexes $[Cr(CO)_2L(\eta^5\text{-}C_5Ph_5)]$ ($L = PMe_3$, PMe_2Ph, $P(OMe)_3$),[32] which have the same basic $[MLL'_2(\eta^5\text{-}L'')]$ piano stool architecture. Spectroelectrochemical CV−IR analysis of a CH_2Cl_2 solution of complex **4** showed, upon cycling between potentials of 0.8 and 1.3 V, production at the electrode of the oxidized species **4**$^+$ ($\nu_{max}(CO) = 2042$ cm^{-1}) with much closer to the expected increase in carbonyl stretching frequency ($\Delta\nu = +100$ cm^{-1}) for a metal-centered one-electron oxidation (Figure 10).[25] This suggests that the *isocloso* distortion likely to be occurring with the complexes **3**$^+$ is probably not happening with complex **4**$^+$. In light of the more powerful donor groups associated with the TMEDA system, this is not altogether surprising.

The disparity in subsequent behavior of complexes **3** and **4** upon electrochemical oxidation is striking. In the oxidized complexes **3**$^+$, the planar 2,2′-bipyridyl ligands afford insufficient steric protection at the metal center from an attacking MeCN nucleophile, such that the ensuing substitution of the carbonyl ligand to give the complexes **3′**$^+$ is rapid. In complex **4**, the metal center clearly benefits from elevated electron donation by the TMEDA ligand, combined with the steric encumbrance of the TMEDA methyl groups. Together,

(30) (a) *Advances in Boron Chemistry*; Siebert, W., Ed.; Royal Society of Chemistry: Cambridge, 1997. (b) *The Borane, Carborane, Carbocation Continuum*; Casanova, J., Ed.; Wiley: New York, 1998. (c) Gallahan, K. P.; Evans, W. J.; Lo, F. Y.; Strouse, C. E.; Hawthorne, M. F. *J. Am. Chem. Soc.* **1975**, *97*, 296. (d) Jung, C. W.; Baker, R. T.; Knobler, C. B.; Hawthorne, M. F. *J. Am. Chem. Soc.* **1980**, *102*, 5782. (e) Jung, C. W.; Baker, R. T.; Hawthorne, M. F. *J. Am. Chem. Soc.* **1981**, *103*, 810. (f) Bould, J.; Greenwood, N. N.; Kennedy, J. D.; McDonald, W. S. *J. Chem. Soc., Chem. Commun.* **1982**, 465. (g) Crook, J. E.; Elrington, M.; Greenwood, N. N.; Kennedy, J. D.; Thornton-Pett, M.; Woollins, J. D. *J. Chem. Soc., Dalton Trans.* **1985**, 2407. (h) Baker, R. T. *Inorg. Chem.* **1986**, *25*, 109. (i) Johnston, R. L.; Mingos, D. M. P. *Inorg. Chem.* **1986**, *25*, 3321. (j) Johnston, R. L.; Mingos, D. M. P.; Sherwood, P. *New J. Chem.* **1991**, *15*, 831. (k) Bould, J.; Rath, N. P.; Barton, L. *Organometallics* **1995**, *14*, 2119. (l) Pisareva, I. V.; Chizhevsky, I. T.; Petrovskii, P. V.; Bregadze, V. I.; Dolgushin, F. M.; Yanovsky, A. I. *Organometallics* **1997**, *16*, 5598. (m) Lei, X.; Shang, M.; Fehlner, T. P. *Inorg. Chem.* **1998**, *37*, 3900. (n) Weller, A. S.; Shang, M.; Fehlner, T. P. *Organometallics* **1999**, *18*, 853.

(31) (a) Attfield, M. J.; Howard, J. A. K.; Jelfs, A. N. de M.; Nunn, C. M.; Stone, F. G. A. *J. Chem. Soc., Dalton Trans.* **1987**, 2219. (b) Carr, N.; Mullica, D. F.; Sappenfield, E. L.; Stone, F. G. A. *Organometallics* **1992**, *11*, 3697.

(32) Hammack, D. J.; Dillard, M. M.; Castellani, M. P.; Rheingold, A. L.; Rieger, A. L.; Rieger, P. H. *Organometallics* **1996**, *15*, 4791.

Table 4. UV−Vis Absorption and Photoluminescence Data

	λ_{max}/nm ($\epsilon \times 10^{-3}$/M^{-1} cm^{-1})[a]			photoluminescence of compd **4**[a,b]		
compd	MeCN	CH_2Cl_2	toluene	solvent	λ_{ex}/nm	λ_{em}/nm
3a	244 (15.8), 282 (11.7), 311 (7.4), 345 (3.7), 440 (0.9)	245 (17.9), 286 (15.5), 310 (sh), 370 (4.5), 457 (1.0)	294 (14.1), 386 (3.6), 496 (1.2)	THF	296	360[c]
3b	269 (15.2), 282 (16.4), 312 (10.2), 350 (5.2), 434 (1.1)	246 (22.8), 287 (20.9), 312 (sh), 364 (5.8), 442 (1.3)	291 (14.8), 379 (4.2), 480 (1.0)	MeTHF[d]	290	450[e]
3c	245 (22.2), 280 (15.8), 310 (10.9), 350 (5.0), 450 (1.0)	246 (21.2), 287 (20.7), 313 (sh), 365 (5.5), 455 (1.2)	292 (20.3), 385 (5.5), 482 (1.4)			
4	253 (8.6), 295 (1.3), 336 (0.9), 477 (0.1)	253 (9.4), 295 (1.4), 336 (1.2), 473 (0.2)	300 (1.0), 332 (0.8), 478 (0.1)			

[a] Measured at 298 K unless otherwise stated. [b] Measured on a 0.5 mM solution unless otherwise stated. [c] Vibronic structure, $\Delta\nu \approx 1000$ cm^{-1}. [d] Measured at 77 K on a 50 μM solution. [e] Single-exponential decay lifetime, $\tau = 0.77$ ms measured at $\lambda_{em} = 446$ and 550 nm.

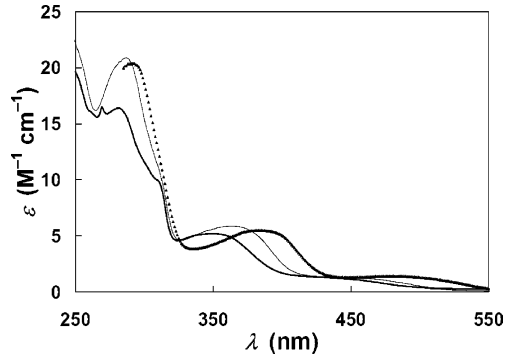

Figure 11. UV−vis absorption spectra for complex **3c**, measured in MeCN (thick line), CH_2Cl_2 (thin line), and toluene (thick dotted line).

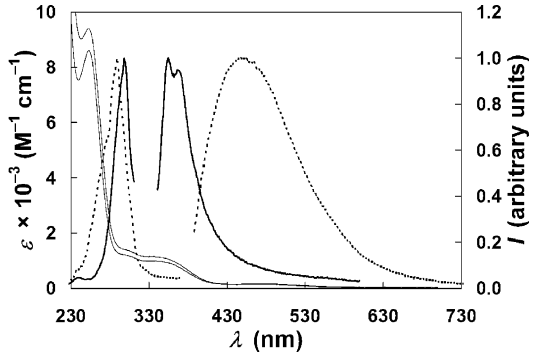

Figure 12. UV−vis absorption spectra (thin lines) for complex **4**, measured in MeCN and CH_2Cl_2 (left ordinate). Photoexcitation and emission spectra measured in THF (0.5 mM) at 298 K (thick lines) and in MeTHF (50 μM) at 77 K (hashed lines) (right ordinate). Solvent-shifted Raman bands have been omitted.

these effects render the metal center almost completely nonlabile under the conditions of the measurement.

Photophysical Chemistry. One motivation for synthesizing this class of ruthenacarborane complexes was to examine the impact of the carborane ligand on the electronic and possible photophysical activity of the Ru−2,2′-bipyridyl system. The complexes are subject to two competing phenomena promoted by the carborane cage: the 2− charge of the $[\eta^5\text{-}C_2B_9H_{11}]^{2-}$ cage ligand could elevate the level of electron density on the metal (i.e., maintain high-energy d orbitals) or this effect could be offset more than sufficiently by the capacity for the cage to delocalize charge about the *closo*-3,1,2-RuC_2B_9 framework. Analysis of the electronic absorption spectra (Table 4) of the complexes **3** helped answer this question. The series of spectra measured in MeCN, CH_2Cl_2, and toluene solutions of complex **3c** are shown in Figure 11 and are representative for all three complexes **3**. Aside from strong ligand-based absorptions below 300 nm, broad, intermediate-strength absorption bands appear at 350 nm ($\epsilon = 5000$ M^{-1} cm^{-1}) and 450 nm ($\epsilon = 1000$ M^{-1} cm^{-1}) for complex **3c** (for example) and they are clearly red-shifted as solvent polarity is decreased (365 nm (CH_2Cl_2), 386 nm (toluene) for the stronger absorption; 455 nm (CH_2Cl_2), 480 nm (toluene) for the weaker absorption). These are very much indicative of charge transfer and d−d bands, respectively, both with heavy metal−ligand orbital mixing, itself a consequence of substantial π interaction between the metal and cage and of course with the CO ligand. The intensity of the stronger, higher-energy absorption suggests that it may be ascribed to the 2,2′-bipyridyl ligand, and it should be noted that a similar transition is conspicuously absent for complex **4**. The electronic absorption spectrum for this latter species, complex **4** (Figure 12), instead revealed two weaker absorptions at 290 nm ($\epsilon = 1300$ M^{-1} cm^{-1}) and 338 nm ($\epsilon = 900$ M^{-1} cm^{-1}), which appear to be much less dependent on solvent polarity. Also observed is a very weak, broad d−d band centered at 477 nm ($\epsilon = 100$ M^{-1} cm^{-1}). Further understanding of the observed electronic spectra for **3** and **4** may be achieved with the assistance of a qualitative MO diagram (Scheme 2). It has been long established by EHMO (extended Hückel molecular orbital) calculations that the $[nido\text{-}7,8\text{-}C_2B_9H_{11}]^{2-}$ anion possesses two highest occupied molecular orbitals, very close in energy, and with facial π symmetry.[33] Thus, we can consider the cage as a π-donor ligand, much like the halide ions of $[Ru(X)(R)(CO)_2L_2]$ (X = Cl, Br; R = alkyl; L_2 = α-diimine, e.g. 2,2′-bipyridyl), upon which the MO energy level diagram in Scheme 2 is modeled.[34] The cage interaction with a *fac*-$[Ru(CO)L_2]^{2+}$ (L_2 = 2,2′-bipyridyl or TMEDA) fragment may then be crudely probed. Using the *x*,*y*,*z*-coordinate scheme of Stufkens et al.,[34] the d_{xy} and d_{xz} orbitals may be expected to be somewhat stabilized relative to the d_{yz} owing to more favorable π-interactions with the carbonyl ligand. The d_{xy} and d_{xz} orbitals have been utilized in bonding with the cage orbitals to give pairs of d−π_{cage} bonding and d−π^*_{cage} antibonding orbitals, leaving the d_{yz} unperturbed by the carborane cage, although some contribution from the 2,2′-

(33) (a) Hamilton, E. J. M.; Welch, A. J. *Polyhedron* **1990**, *9*, 2407. (b) Mingos, D. M. P.; Forsyth, M. I.; Welch, A. J. *J. Chem. Soc., Dalton Trans*. **1978**, 1363.

(34) Nieuwenhuis, H. A.; Stufkens, D. J.; Oskam, A. *Inorg. Chem*. **1994**, *33*, 3212.

Scheme 2. Qualitative MO Diagram for the Frontier Orbitals of Complexes **3** and **4**[a]

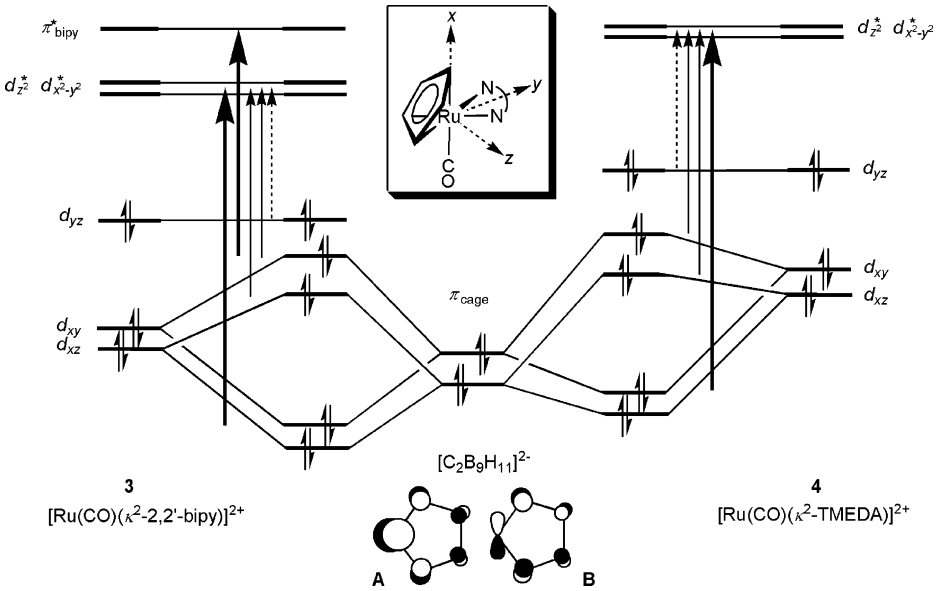

[a] MOs for $[C_2B_9H_{11}]^{2-}$ taken from ref 33.

bipyridyl nitrogens to the latter might obviously be expected. The EPR analysis following oxidation of complex **4** provides strong evidence for this last hypothesis (vide supra). For complex **3c**, there may be no substantial difference in energy here, as suggested by the lack of observation of a distinguishable d−d band, i.e., such a band may be masked by the d$-\pi^*_{cage}$ → d* transitions. The intermediate strength band at 350 nm may then be ascribed to a d$-\pi^*_{cage}$ → π^*_{bipy} process, likely emanating from the $d_{xy}-\pi^*_{cage}$ orbital, since an electronic transition from the d_{yz} orbital should be overlap-forbidden. Because the energy of this transition is high for such a charge-transfer excitation, one assumes that the π^*_{bipy} energy level lies at or above the highest-energy d orbitals (actually labeled d*, as they are no doubt the antibonding product resulting from relatively strong σ interactions between the metal and the carborane cage ligand). This is also supported by the EPR measurements carried out following one-electron reduction of complex **3c** (vide supra). It is also feasible that this stronger transition itself masks another d$-\pi^*_{cage}$ → d* band. This is because there are two such bands for complex **4** (290 and 338 nm) for which the d$-\pi^*_{cage}$ → π^*_{bipy} process should now of course be absent. The d orbitals for complex **4** may be expected to lie toward higher energy with the more powerful TMEDA donor present, particularly the d* orbitals, which may now result in the d$-\pi^*_{cage}$ → d* bands being discernible from the d−d band as observed. Poorer overlap between the d_{xy}, d_{xz} orbitals with those of the cage may also account for lower wavelength dependency on solvent polarity. For complexes **3** and **4**, bands at ca. 310 nm (**3**) and 253 nm (**4**) are tentatively ascribed to LMCT transitions. They are similarly intense (ϵ = 7400−10 900 (**3**), 8600 (**4**) M^{-1} cm^{-1}) and virtually invariant with solvent polarity, although in the case of complexes **3**, discernment from 2,2′-bipyridyl-centered $\pi-\pi^*$ transitions is difficult.

The electronic configuration displayed in Scheme 2 may also account for a lack of observed photophysical activity for the complexes **3**. If the π^*_{bipy} energy level is indeed sufficiently high-lying, nonradiative ligand-field pathways will be readily energy-accessible and no MLCT-type emission should be observed. Examination for photoluminescence in solutions at ambient temperatures and in low-temperature glasses bore this suspicion out, although the low-temperature measurements showed evidence of weak $\pi-\pi^*$ emissions, likely 2,2′-bipyridyl-centered. Complex **4**, on the other hand, exhibited quite unexpected photophysical behavior, and preliminary studies are presented here.

In THF at ambient temperatures, complex **4** is weakly emissive in the near-UV (λ_{em} = 360 nm, $\Phi < 10^{-4}$) with excitation at λ_{ex} = 296 nm (Table 4, Figure 12). The emission spectrum is very similar in appearance and intensity in CH_2Cl_2 solution, and although MeCN solutions showed some activity at the same wavelengths, it was considerably weaker. These results prompted analysis in MeTHF glass at 77 K with results also given in Table 4 and shown in Figure 12. Excitation is shifted only slightly from that at 298 K (λ_{ex} = 290 nm), but a much more intense, broad, unstructured blue emission centered at λ_{em} = 450 nm becomes apparent. This represents a large change in Stokes shift from 5400 cm^{-1} at room temperature to 12 600 cm^{-1} at 77 K, suggesting phosphorescence in the low-temperature MeTHF glass is predominant. Emission decay analysis (Figure 13) yielded a single-exponential lifetime, τ_{450} = 0.77 ms, which was the same in the emission tail (λ_{em} = 550 nm) as at the peak. The source of the emission is cause for ongoing inquiry, but it seems that with clearly observable d−d states in the electronic absorption spectrum, some kind of structural geometric adjustment must be occurring to facilitate such luminescence, which bears an uncanny resemblance to a typical d−d phosphorescent state,[35] and would be highly unusual for a Ru^{II} center.[35c] This assertion may be supported

(35) (a) Watts, R. J. *Inorg. Chem.* **1981**, *20*, 2302. (b) Huang, W. L.; Segers, D. P.; DeArmond, M. K. *J. Phys. Chem.* **1981**, *85*, 2080. (c) Segers, D. P.; DeArmond, M. K. *J. Phys. Chem.* **1982**, *86*, 3768.

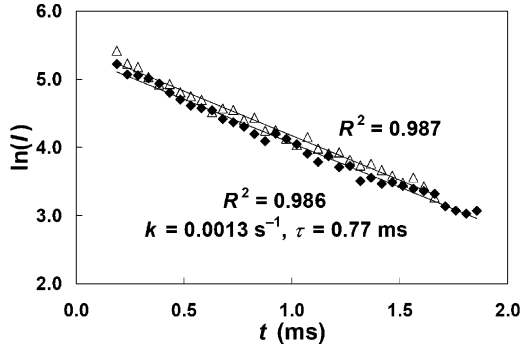

Figure 13. Photoemission decay analysis for complex **4** in MeTHF (50 μM) at 77 K: at $\lambda_{em} = 450$ nm (△); at $\lambda_{em} = 550$ nm (◆).

Scheme 3. Photochemical and -physical Excitation of Complex **4**

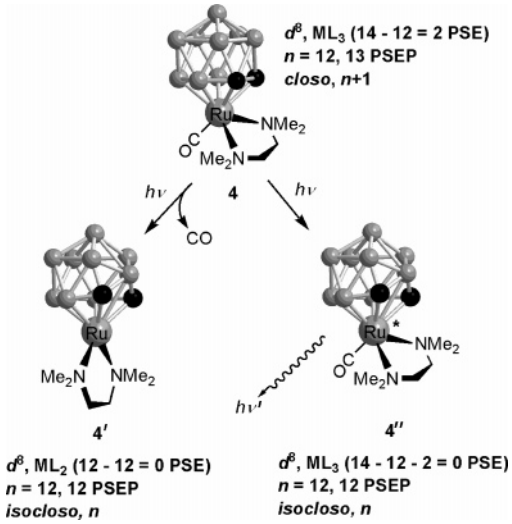

by a degree of excitation/emission peak asymmetry, especially for the low-temperature data, even when spectra are more appropriately compared on an energy scale (Supporting Information, Figure S6). Time-based intensity measurements at 77 and 298 K verified that emission did not increase, so that the chromophore is itself not likely a product of photolysis. Indeed, preliminary IR measurements of a photolyzed **4a**/MeTHF matrix at 77 K suggested the only photoproduct from such excitation results from CO dissociation to give a 16-electron complex [3,3-{κ^2-$Me_2N(CH_2)_2$-NMe_2}-*closo*-3,1,2-$RuC_2B_9H_{11}$] **4′**, reminiscent of the cyclopentadienide complexes [Ru(η^5-C_5R_5){κ^2-$Me_2N(CH_2)_2$-NMe_2}]$^+$ mentioned above (Scheme 3). In hypothesizing what the emissive species is, one is reminded of basic Wade−Mingos rules for metallacarborane electronic structures.[26] If one considers elevating a relatively energetic cage-bonding electron to a cage-antibonding orbital in a 13 (n + 1) PSEP *closo* icosahedron, then the PSEP count formally decreases by one pair, the consequence of which should be a structural adjustment to a 12 (n) PSEP *isocloso* species. In previously characterized ground-state 12-vertex complexes with this configuration, the cage C−C connectivity is ruptured and the 6-B atom from the upper pentagonal belt migrates to within bonding distance of the metal vertex to give an apparent η^6-cage coordination.[31] The emissive excitation appears coincident with one of the two weak-intermediate absorptions identified as those resulting from d−π^*_{cage} antibonding orbitals (Scheme 2). One of these, formed from the cage π orbital **A**, is bonding with respect to the cage C−C connectivity, while the other, formed from **B**, is antibonding. Depopulation of the former only may be sufficient to initiate the C−C rupture expected in a *closo* → *isocloso* transformation, which is implicated in the observed phosphorescence of complex **4** (Scheme 3). While the 77 K emission is broad and featureless, supporting geometric rearrangement, some unresolved fine structure is apparent in the excitation spectrum. More evident is the vibronic structure ($\Delta\nu \approx 1000$ cm^{-1}) in the 298 K emission spectrum, which does correspond in energy to carborane cage breathing vibrational modes.[36] Pulsed excitation measurements suggested the lifetime $\tau_{360} < 1$ μs, and unfortunately, currently available instrumentation does not permit a more accurate measurement. Thus, assignment of the mode of luminescence cannot be confidently made at this time, although further probative studies will commence shortly. Though we hypothesize in Scheme 3 that an excited-state *isocloso* species, **4″**, is structurally analogous to the electrochemically generated systems described above (and those in turn were based on the X-ray structural characterizations of Stone et al.[31]), there is no direct evidence that it will actually have the same prototypical structure with regard to the 6-B migration toward the metal vertex. However, it seems that if some inner-sphere reorganization is required to account for the photophysical behavior, then it is better to err on the side of structural precedent and our own evidence from the spectroelectrochemical studies described here. Ironically, accounting for the lack of photoactivity of complexes **3** consequently becomes an additional challenge. However, one may surmise that the stability conferred upon the oxidized species **4**$^+$ over that of complexes **3**$^+$ may also be responsible for the apparent decrease in efficiency of nonradiative decay of the distorted excited state of complex **4** versus a similarly stimulated complex **3**. In understanding this, one should be cognizant of the fact that an excitation to give an n PSEP *isocloso* species may be conceived as being more structurally aggressive than an oxidation to yield an n + 0.5 PSEP moiety.

Conclusions

A novel class of ruthenacarborane complexes has been developed, and although the 2,2′-bipyridyl-based complexes **3** are photophysically inactive, their substitution lability upon electrochemical oxidation may be used to further synthetic advantage as a means of introducing stronger donor ligands (e.g., phosphines, nitriles, isonitriles, etc.) to replace the strongly π-acidic carbonyl. This in turn leads to the prospect of an expanding family of such complexes, which may display more illuminating photophysical characteristics. The substitution inertness of the TMEDA complex **4** following oxidation, on the other hand, provides a stark contrast to complexes **3**, with the stronger donor capacity and steric congestion afforded by the methyl groups of the TMEDA ligand in complex **4** accounting for its enhanced electrochemical stability. A *closo* → *isocloso* metamorphosis has

(36) (a) Leites, L. A. *Chem. Rev.* **1992**, *92*, 279. (b) Salam, A.; Deleuze, M. S.; François, J.-P. *Chem. Phys.* **2003**, *286*, 45.

been invoked for the cationic intermediates $\mathbf{3}^+$, and experiments to isolate a putative *isocloso* $n + 0.5$ PSEP complex are progressing. The luminescent behavior of complex **4** was surprising, and its origin remains under investigation, although we hypothesize that a *closo* → *isocloso* transformation is once again involved with the emissive behavior. Further studies to modify the complex architecture, such as tethering the cage carbon vertexes together, and to examine the effect on photophysical behavior are under way.

Experimental Section

General Considerations. Solvents (CH_2Cl_2, hexanes, MeCN, THF, MeTHF) were distilled over appropriate drying agents under argon prior to use. All reactions were carried out under a dry, oxygen-free argon atmosphere using Schlenk line and glovebox techniques. The reagents 2,2′-bipyridyl, 4,4′-di-*t*-butyl-2,2′-bipyridyl, 4,4′-di-*n*-nonyl-2,2′-bipyridyl, *N*,*N*,*N*′,*N*′-tetramethylethylenediamine, and *tris*(4-bromophenyl)ammoniumyl hexachloroantimonate were purchased from Aldrich and used as received. Complex **1** was prepared using the literature method,[6a] as was a THF solution of sodium naphthalenide.[37] Chromatography columns (ca. 15 cm in length and 3 cm in diameter) were packed with silica gel (Aldrich, 70−230 mesh).

Instrumentation. All solution measurements were made at 298 K unless otherwise stated. IR measurements were made using solution cells in a Perkin-Elmer RX-I FTIR spectrometer. NMR measurements were recorded using a Varian Gemini 300 MHz spectrometer: ^{1}H (300.0 MHz); ^{13}C (75.4 MHz); ^{11}B (96.3 MHz). X-band EPR measurements were made using a Bruker-EMX spectrometer with a modulation frequency of 100.000 kHz and a modulation amplitude of 1.000 G. The simulated solution EPR spectrum of the oxidation product of complex **4** was calculated using the Bruker SimFonia software bundled with the WINEPR instrument operating software, which employed directly imported experimental parameters. Electrochemical experiments were performed with a CH Instruments CHI620B electrochemical analyzer. All potentials were recorded and quoted relative to an $Ag/AgNO_3$ (MeCN, 10 mM) reference electrode at 298 K. All solutions were studied in a three-electrode cell under Ar in distilled, deoxygenated solvents and contained 0.1 M $[NBu^n_4][PF_6]$ as supporting electrolyte in either CH_2Cl_2 or MeCN. All measurements were made on a glassy carbon disk working electrode with a surface area of 7.07 mm^2, which was frequently polished, rinsed, and dried between measurements. The Pt wire counter electrode was precleaned by soaking in concd HNO_3, rinsed with distilled water, and then flame-dried. Cyclic voltammetry (CV) experiments were run with 1.0 mV sample intervals and typically with a sensitivity of 10 μA V^{-1}. CV experiments were run both with initial positive and negative polarities and showed little variation with this parameter. Chronoamperometry (CA) experiments were also run with the same electrodes. A two-step procedure with optimum pulse widths, $\tau =$ 0.5−1.0 s, and a sample interval of 1 mV were carried out. Sensitivity was set at 0.1 mA V^{-1}. Digital simulations were carried out using DigiElch employing measured experimental parameters (concentrations, working electrode surface area, electrode potentials, scan rates, etc.).[38] Diffusion coefficients were taken from Cottrell plots of chronoamperometric data where possible; otherwise, reasonable estimates were used following exhaustive fitting. The default modeling parameters were employed. UV−vis spectral measurements (800 → 220 nm) were made with a Shimadzu 2530 UV−visible absorption spectrophotometer. Photoluminescence measurements were made with a Photon Technologies QM4 fluorescence spectrophotometer with a Xe arc lamp light source and digital PMT detector. Emission and reference source gain excitation corrections were applied to all steady-state data. Slit widths were typically set at 5 nm. Appropriate cutoff filters were used to eliminate peaks due to solvent Raman-shifted bands and excitation harmonics when possible. Solution samples at ambient temperatures were measured in a quartz sample cuvette with Schlenk attachment to deoxygenate samples. Samples measured at 77 K were degassed and analyzed in a quartz NMR tube with Schlenk attachment and set in a quartz-bottomed Dewar flask in an argon-filled sample chamber. Excited-state decay measurements were made using a Xe flash lamp. Data were collected over 100 channels and with an integration time of 50 μs. A total of 25 shots were taken at a frequency of 10 Hz for each data point, and the total decay was then averaged over three experimental runs, without an instrument response function. Spectroelectrochemical measurements were made on 1.0 mM solutions of complexes **3c** and **4** in CH_2Cl_2 (oxidation) or MeCN (reduction) with 0.1 M $[NBu^n_4][PF_6]$ electrolyte using a Bioanalytical Systems CV50W potentiostat in tandem with a Bruker Vector 22 FTIR spectrometer equipped with a mid-IR fiber-optic dip probe and liquid-nitrogen-cooled MCT detector (RemSpec Corporation, Sturbridge, MA). Details of the experimental setup and procedure have been previously published.[39] Stacked CV−IR spectra were measured over the first minute of the stimulated redox process with sampling times of 4−8 s.

X-Ray Crystallography. Crystals were mounted onto glass fibers in a random orientation. Preliminary examination and data collection were performed using a Siemens SMART charge-coupled device (CCD) detector system single-crystal X-ray diffractometer equipped with a sealed-tube X-ray source using graphite-monochromated Mo Kα radiation ($\lambda = 0.71073$ Å). Preliminary unit cell constants were determined with a set of 45 narrow-frame scans (0.3° in ω). A total of 4026 frames of intensity data were collected at a crystal-to-detector distance of 4.91 cm. The double-pass method of scanning was used to reduce noise. The collected frames were integrated using an orientation matrix determined from the narrow-frame scans. The SMART software package was used for data collection, and SAINT[40] was used for frame integration. Analysis of the integrated data did not show any decay. Final cell constants were determined by a global refinement of the *x*, *y*, *z* centroids of thresholded reflections from the entire dataset. Absorption corrections were applied to the data using equivalent reflections (SADABS).[41] The SHELX-97[42] software package was used for structure solutions (by direct methods) and refinement. Full-matrix least-squares refinement was carried out by minimizing $\sum w(F_o^2 - F_o^2)^2$. The non-hydrogen atoms were refined anisotropically to convergence. Noncage hydrogen atoms were included in calculated positions and treated using appropriate riding models. Cage hydrogens were located from the difference Fourier map and included in the final refinement. The structure refinement parameters are given in Table 5, and selected bond angles and distances are given in the legends for Figures 1 (**3a**) and 2 (**4**). A complete list of positional and isotropic displacement coefficients for the hydrogen atoms, anisotropic displacement coefficients for the non-

(37) Connelly, N. G.; Geiger, W. E. *Chem Rev.* **1996**, *96*, 877.
(38) Rudolph, M. *DigiElch* ver. 2.0; Friedrich-Schiller-Universität: Jena, Germany, 2005.
(39) Shaw, M. J.; Henson, R. L.; Houk, S. E.; Westhoff, J. W.; Jones, M. W.; Richter-Addo, G. B. *J. Electroanal. Chem.* **2002**, *534*, 47.
(40) Bruker Analytical X-ray, Madison, WI, 2002.
(41) Blessing, R. H. *Acta Cryst.* **1995**, *A51*, 33.
(42) Sheldrick, G. M. *SHELX-97*; University of Göttingen: Göttingen, Germany, 1997.

Table 5. Crystallographic Data

	3a	4
empirical formula	$C_{13}H_{19}B_9N_2ORu$	$C_9H_{27}B_9N_2ORu$
fw	417.66	377.69
cryst dimens (mm^3)	0.06 × 0.17 × 0.21	0.10 × 0.13 × 0.18
cryst color, shape	yellow, parallelepiped	orange, rectangular prism
cryst syst, space group	monoclinic, $P2_1/n$	orthorhombic, $P2_12_12_1$
a (Å)	7.5955(2)	8.81550(10)
b (Å)	21.3584(6)	13.1217(2)
c (Å)	11.0440(3)	15.2641(2)
β (deg)	102.502(1)	
V (Å^3)	1749.16(8)	1765.67(4)
Z	4	4
D_{calcd} (g cm^{-3})	1.586	1.421
μ(Mo Kα) (mm^{-1})	0.899	0.882
T (K)	170(2)	293(2)
θ range (deg)	1.91−27.50	2.05−27.99
reflns collcted	22 733	23 686
independant reflns (R_{int})	4007 (0.0395)	4227 (0.0480)
wR2, R1[a] ($I > 2\sigma(I)$)	0.0891, 0.0530	0.0806, 0.0530
wR2, R1[a] (all data)	0.0911, 0.0594	0.0812, 0.0554
absolute structure param	−	0.03(6)
GOF on F^2	1.237	1.288
largest diff. peak and hole (e Å^{-3})	0.807, −1.377	0.695, −1.309

[a] Refinement was block full-matrix least-squares on all F^2 data: $wR2 = [\sum\{w(F_o^2 - F_c^2)^2\}/\sum w(F_o^2)^2]^{1/2}$ where $w^{-1} = \sigma^2(F_o^2)$. The value $R1 = \sum||F_o| - |F_c||/\sum|F_o|$.

hydrogen atoms, and bond distances and angles are available in CIF format as Supporting Information. CCDC 277842 and 277843 contain the supplementary crystallographic data for this paper. These data can be obtained free of charge from The Cambridge Crystallographic Data Centre via www.ccdc.cam.ac.uk/data_request/cif.

Synthesis of [3-CO-3,3-{κ^2-2,2′-$(NC_5H_4)_2$}-*closo*-3,1,2-$RuC_2B_9H_{11}$]. The reagent **1** (0.20 g, 0.63 mmol), 1 mol equiv of 2,2′-bipyridyl (0.10 g, 0.63 mmol) and 2 mol equiv of Me_3NO (0.10 g, 1.26 mmol) were combined in a 200 mL three-neck round-bottom flask, fitted with a stopcock and stirrer bar. To this flask was added MeCN (70 mL), and the reaction mixture stirred. Upon the addition of solvent, the solution became a deep brown/orange and CO_2 and NMe_3 gases were rapidly evolved and vented into a fume hood. The solution was stirred for 12 h with monitoring by FTIR spectral measurements. Upon complete consumption of complex **1**, solvent was removed in vacuo and then silica gel (ca. 0.5 g) and CH_2Cl_2 (5 mL) added to the residue. Solvent was once again removed in vacuo with vigorous stirring to preadsorb the reaction mixture components onto the silica gel. The solid preadsorbate was then chromatographed, the initial elution with CH_2Cl_2/hexanes (4:1) yielding a bright yellow-orange band. As this fraction was removed from the column, the polarity of the solvent mixture was gradually increased to a combination of 1:1. Solvent was removed in vacuo, and recrystallization from CH_2Cl_2/hexanes (10 mL, 1:1) afforded yellow-orange microcrystals of [3-CO-3,3-{κ^2-2,2′-$(NC_5H_4)_2$}-*closo*-3,1,2-$RuC_2B_9H_{11}$] (**3a**) (0.06 g), which were dried in vacuo.

Synthesis of [3-CO-3,3-{κ^2-4,4′-$((CH_2)_8Me)_2$-2,2′-$(NC_5H_3)_2$}-*closo*-3,1,2-$RuC_2B_9H_{11}$]. Using the same procedure, reaction of complex **1** (0.20 g, 0.63 mmol), 4,4′-di-*n*-nonyl-2,2′-bipyridyl (0.26 g, 0.63 mmol) and Me_3NO (0.10 g, 1.26 mmol) yielded yellow microcrystals of [3-CO-3,3-{κ^2-4,4′-$((CH_2)_8Me)_2$-2,2′-$(NC_5H_3)_2$}-*closo*-3,1,2-$RuC_2B_9H_{11}$] (**3b**) (0.09 g).

Synthesis of [3-CO-3,3-{κ^2-4,4′-Bu^t_2-2,2′-$(NC_5H_3)_2$}-*closo*-3,1,2-$RuC_2B_9H_{11}$]. Using the same procedure, reaction of complex **1** (0.25 g, 0.79 mmol), 4,4′-di-*t*-butyl-2,2′-bipyridyl (0.21 g, 0.79 mmol), and Me_3NO (0.12 g, 1.57 mmol) yielded yellow microcrystals of [3-CO-3,3-{κ^2-4,4′-Bu^t_2-2,2′-$(NC_5H_3)_2$}-*closo*-3,1,2-$RuC_2B_9H_{11}$] (**3c**) (0.20 g).

Synthesis of [3-CO-3,3-{κ^2-$Me_2N(CH_2)_2NMe_2$}-*closo*-3,1,2-$RuC_2B_9H_{11}$]. Using a similar procedure (but with addition of TMEDA shortly after MeCN), reaction of complex **1** (0.20 g, 0.63 mmol), *N*,*N*,*N*′,*N*′-tetramethylethylenediamine (95 μL, 0.63 mmol), and Me_3NO (0.10 g, 1.26 mmol) afforded deep orange microcrystals of [3-CO-3,3-{κ^2-$Me_2N(CH_2)_2NMe_2$}-*closo*-3,1,2-$RuC_2B_9H_{11}$] (**4**) (0.10 g).

Reduction of Complex 3c with Sodium Naphthalenide. A 94 mM solution of $NaC_{10}H_8$ (200 μL, 0.019 mmol) in THF was transferred to a sample of complex **3c** (0.010 g, 0.019 mmol) in an NMR−Schlenk vessel maintained under Ar. The NMR tube was capped under the Ar stream, then sealed with a Teflon tape wrap following removal from the Schlenk tube and agitated. The sample was stable for ≥12 h and subjected to immediate EPR measurement. Solid-state samples were produced by careful removal of solvent in vacuo and pumping for 2−3 h, following replacement of the NMR tube in the NMR−Schlenk vessel and decapping.

Oxidation of Complex 4 with $[N(C_6H_4Br\text{-}4)_3][SbCl_6]$. Using a similar method, a 24 mM solution of $[N(C_6H_4Br\text{-}4)_3][SbCl_6]$ (500 μL, 0.012 mmol) in CH_2Cl_2 was transferred to a sample of complex **4** (0.005 g, 0.013 mmol), the resulting solution being stable for ≥24 h. The solution was subjected to EPR measurement, following which, solvent was carefully removed in vacuo as above, washing the residue with CH_2Cl_2/Et_2O × 3 (1:1) and then pumping for 2−3 h. The resulting microcrystals were used for a solid-state EPR measurement.

Acknowledgment. This work was supported by funding from the Saint Louis University Beaumont Faculty Development Fund, and funding from Research Corporation (Cottrell Grant No. CC5748) is also acknowledged for the purchase of the fluorescence spectrophotometer. P.A.J. thanks Drs. Shelley Minteer and Steven Buckner (Saint Louis University) for helpful discussions. The preliminary frozen matrix photolysis study of complex **4** was carried out by Dr. Tom Bitterwolf (Univesirty of Idaho), and a full publication of these results will be forthcoming.

Supporting Information Available: Figures S1−S6. Tables of crystallographic data, including fractional coordinates, bond lengths and angles, anisotropic displacement parameters, and hydrogen atom coordinates, of **3a** and **4** through combined CIF files. This material is available free of charge via the Internet at http://pubs.acs.org.

IC051463E